

# Final Year Report

---



Project Title: **Battery Embedded Energy Storage System for Stabilization of Renewable Energy in PSMG Wind Turbine**

Project type: **Final Year Undergraduate Project 2019/20**

Student name: **Raymond Zhen**

Programme of study: **BEng FT Electrical & Electronic Engineering 4 year with IE**

Email: **r.zhen@se16.qmul.ac.uk**

Project Supervisor: **Dr Kamyar Mehran**

## Abbreviations

| Abbreviation | Definition                                  |
|--------------|---|
| BMS          | Battery management system                   |
| EES          | Embedded energy storage                     |
| SOC          | State of Charge                             |
| SOH          | State of Health                             |
| OCV          | Open circuit voltage                        |
| NTC          | Negative temperature co-efficient           |
| PCB          | Printed circuit board                       |
| I2C          | Inter-inter communication                   |
| UART         | Universal asynchronous receiver-transmitter |
| AFE          | Analog front end (referring to BQ chip)     |
| FSM          | Finite State Machine                        |
| ADC          | Analog to digital converter                 |

## List of Figures

|    |  |    |
|----|--|----|
| 1  | Grid Structure [1]                               | 11 |
| 2  | Typical model of PSMG wind turbines              | 12 |
| 3  | Proposed Simulation Model Structure              | 12 |
| 4  | Wind Turbine Generic Power Curve                 | 13 |
| 5  | Wind turbine simulation model                    | 14 |
| 6  | Bi-directional Converter Model                   | 17 |
| 7  | Single Lithium ion model plot with Simulink      | 18 |
| 8  | Model of Battery Housing                         | 21 |
| 9  | Housing the Battery Bank within Wind Turbine     | 21 |
| 10 | Render of Full Turbine                           | 22 |
| 11 | Microchip products                               | 24 |
| 12 | Block Diagram of system                          | 24 |
| 13 | Flowchart of Firmware                            | 26 |
| 14 | Watchdog Timer Parallel process                  | 27 |
| 15 | I2C Communication example cited from TI[2]       | 28 |
| 16 | I2C Communication write byte stream              | 28 |
| 17 | OCV Graph  | 30 |
| 18 | NTC thermistor curve                             | 32 |
| 19 | Components of the BMS Hardware                   | 33 |
| 20 | Recommended PCB Layout                           | 34 |
| 21 | PCB Layout in Altium                             | 34 |
| 22 | Current Sense Resistor Circuit with Filtering    | 35 |
| 23 | Cell-balancing & Monitoring                      | 36 |
| 24 | Charge & Discharge Mosfets                       | 36 |
| 25 | Latching Circuit                                 | 37 |
| 26 | Latching Circuit Simulation Results              | 38 |
| 27 | Simulation results using real wind profile       | 39 |
| 28 | Simulation results using real wind profile       | 40 |
| 29 | Occurrence of coarse oscillation                 | 41 |
| 30 | SOC of battery bank with varying wind speeds     | 41 |
| 31 | Viewing data on GUI from BMS                     | 42 |
| 32 | Hardware Demo & Prototype                        | 42 |
| 33 | Simulated vs Sampled data readings               | 43 |
| 34 | Samsung INR18650 Nominal specification datasheet | 58 |

## List of Tables

|   |   |    |
|---|---|----|
| 1 | PSMG Wind Turbine Model Simulation Parameters | 14 |
| 2 | Buck Converter Calculations                   | 15 |
| 3 | Boost Converter Calculations                  | 16 |
| 4 | Boost Converter Calculations                  | 23 |
| 5 | BMS Features                                  | 25 |
| 6 | Pin definition for PIC16F1719                 | 25 |
| 7 | Recorded parameters of RS PRO NTC thermistor  | 31 |
| 8 | BMS Requirements Met                          | 44 |

# Contents

|   |           |
|---|-----------|
| <b>Abstract</b>   | <b>5</b>  |
| <b>Acknowledgements</b>   | <b>6</b>  |
| <b>1 Introduction</b>   | <b>7</b>  |
| 1.1 Background . . . . .  | 7         |
| 1.1.1 Re-chargeable batteries . . . . .   | 7         |
| 1.1.2 Battery management systems . . . . .  | 8         |
| 1.2 Problem statement . . . . .   | 8         |
| 1.3 Aim . . . . .   | 8         |
| 1.4 Objectives . . . . .  | 8         |
| <b>2 Literature Review</b>  | <b>10</b> |
| 2.1 Current approaches . . . . .  | 10        |
| 2.1.1 Microgrids . . . . .  | 10        |
| 2.1.2 Academic Research . . . . .   | 10        |
| 2.1.3 Line-Interactive UPS . . . . .  | 11        |
| <b>3 Simulink Modelling</b>   | <b>12</b> |
| 3.1 Proposed Model Design . . . . .   | 12        |
| 3.2 Wind Turbine Model . . . . .  | 12        |
| 3.2.1 Theoretical Approximation & Considerations . . . . .                        | 12        |
| 3.2.2 Simulation Model . . . . .  | 13        |
| 3.3 Bi-directional Converter Design . . . . .                                     | 14        |
| 3.3.1 Specifications . . . . .  | 15        |
| 3.3.2 Model . . . . .   | 16        |
| 3.4 Battery Model and Choice . . . . .  | 17        |
| <b>4 3D Modelling</b>   | <b>20</b> |
| 4.1 Model Motivation . . . . .  | 20        |
| 4.2 Software package . . . . .  | 20        |
| 4.3 Justification . . . . .   | 20        |
| <b>5 Battery Management System Design</b>   | <b>23</b> |
| 5.1 Technical Background . . . . .  | 23        |
| 5.1.1 BQ76920 Analogue Front End Chip . . . . .                                   | 23        |
| 5.1.2 PIC16F1719 Micro-controller . . . . .                                       | 23        |
| 5.2 Overview & Specification . . . . .  | 24        |
| 5.2.1 System Block Diagram . . . . .  | 24        |
| 5.2.2 Functionality & Features . . . . .  | 24        |
| 5.3 Pin Definitions . . . . .   | 25        |
| 5.4 Software . . . . .  | 26        |
| 5.4.1 Flow Chart . . . . .  | 26        |
| 5.4.2 Algorithms and Software Design . . . . .                                    | 27        |
| 5.4.2.1 Finite State Machine . . . . .  | 27        |
| 5.4.2.2 Communications with connected devices on bus using I2C protocol . . . . . | 27        |
| 5.4.2.3 Watchdog Timer . . . . .  | 28        |
| 5.4.2.4 SOC estimation and correction . . . . .                                   | 29        |
| 5.4.2.5 NTC thermistor using Stein-hart and Hart approach . . . . .               | 30        |
| 5.4.2.6 Isolated Serial Communication . . . . .                                   | 32        |

|           |  |           |
|-----------|--|-----------|
| 5.5       | Hardware . . . . .   | 33        |
| 5.5.1     | PCB Design . . . . .   | 33        |
| 5.5.2     | Current Sensing Resistor for Coloumb Counting . . . . .              | 34        |
| 5.5.3     | High Power Cell Balancing and Voltage Monitoring Circuit . . . . .   | 35        |
| 5.5.4     | Safety Battery Disconnect using Charge & Discharge Mosfets . . . . . | 36        |
| 5.5.5     | Safety Shutdown Latching Circuit . . . . .                           | 37        |
| <b>6</b>  | <b>Testing &amp; Results</b>   | <b>39</b> |
| 6.1       | Simulation results . . . . .   | 39        |
| 6.2       | Limitation of the simulation model . . . . .                         | 40        |
| 6.3       | Testing the BMS . . . . .  | 41        |
| 6.3.1     | Testing the thermistor . . . . .                                     | 43        |
| <b>7</b>  | <b>Conclusion</b>  | <b>44</b> |
| <b>8</b>  | <b>Future Improvements</b>   | <b>44</b> |
| 8.1       | Simulation . . . . .   | 44        |
| 8.2       | BMS . . . . .  | 44        |
| <b>9</b>  | <b>Appendix - A - Code</b>   | <b>48</b> |
| <b>10</b> | <b>Appendix - B - Schematic</b>                                      | <b>48</b> |
| <b>11</b> | <b>Appendix - C - Models</b>   | <b>53</b> |
| <b>12</b> | <b>Appendix - D - Misc</b>   | <b>56</b> |

## **Abstract**

## Acknowledgements

# 1 Introduction

---

Wind is unpredictable due to natural characteristic which contains both properties wind speed and direction, these affect the integration with the network grid during abnormal wind conditions, in such case, there will be an imbalance with both voltage and frequency generation of the converters. These converters used in wind turbines transform mechanical energy to electrical energy which must match the electrical requirements of the grid, if there is any mismatch, this will lead to destabilisation of wind turbine with the grid, essentially becoming physically disconnected. The nature of wind causes variation in power generation which causes an increase in  $I^2R$  losses in wind farm cables, in extreme cases,  $\approx 50\%$  of power generated from a wind turbine can be lost in cables [3].

There is a steady growth in recent years in the production of medium to large size wind turbines, the average sized wind turbine being manufactured is typically 2.5-3MW which can power 1500 average EU households [4]. To enable high penetration of wind energy we reduce the occurrence of destabilisation with the network grid. Wind power has contributed to 12% in 2016 and 18% in 2018 to all electricity consumed in the UK [5], this source shows that this trend will continue to rise due to the movement towards greener energy and security of supply.

During times where there is a high supply of power being generated and low demand from the population, it is clear that this energy needs to be stored for times where wind power generation is low and demand is high.

A solution to enable high penetration of wind power and security of supply we can introduce Embedded energy storage (EES). EES has been a rising trend in the past decade, EES is a type of device where we can store energy produced by a source and use it at a later time, this is a general form of a battery. It is widely used throughout the world on many devices, for example, mobile phones, we are not limited to small scale storage there has been interest in energy storage for electrical power systems such as storage for renewable energy.

It is possible to realise a rechargeable battery bank within a wind turbine, they may be used with generators such as a permanent magnet synchronous generator (PMSG) or Asynchronous induction generator. Majority of the wind turbines deliver suitable voltage at low wind speeds to charge battery banks, one such example includes the Vestas-V90 which outputs 690V before it is stepped up to match grid voltage [6].

## 1.1 Background

To understand the context of the project, background information is required. The fundamental backbone of an EES is the battery, we will discuss two core components which make up an EES which include re-chargeable batteries and an battery management system.

### 1.1.1 Re-chargeable batteries

Re-chargeable batteries work on a simple concept where electrical energy is converted into chemical energy and stored, which can later be retrieved when connected to a load. With many varieties of battery cells to look at they come with different characteristics, some include capacity(mAh), shape and charge/discharge lifecycles. The following common types of cells are as listed:

1. **Lithium-ion** - a popular choice of energy storage in the current trend used in electric vehicles, prices of lithium ion cells have been rapidly decreasing. The price in 2012 is \$600 per-kilowatt-hour and in 2016 is around \$145 per-kilowatt-hour [7], this makes it an attractive choice for building battery banks for high voltage electric vehicles. Lithium-ion is used where high-energy density and lightweight is the most important attribute in a system.



2. **Nickel-metal hydride** - which abbreviates to Ni-MH, offers higher energy density when compared to Nickel Cadmium cells but at a comprise of reducing charging/discharging cycle. This cell is used in a variety of industrial application such as medical instrument and hybrid cars [8].
3. **Nickel Cadmium** - which abbreviates to Ni-Cd, these cells have been understood quite well as they have been in the used extensively, these cells offer long service life and can discharge a large amount of current, they can withstand extreme temperature and suitable environmental challenges. The application for these cells makes them great for power tools, aviation and uninterruptable power supply (UPS).
4. **Lead Acid** - The lead acid battery is one of the oldest rechargeable battery which was invented in 1859, typically used in automotive applications such as cars as these batteries are rugged and can withstand accidental short circuits. Lead acid brings up environmental concerns as the toxins within the battery cannot be disposed of in landfills. In situations where systems require low cost, robustness and weight not being of importance, the lead acid battery can be considered.

### 1.1.2 Battery management systems

A battery management system is an electronic device which provides protect battery from operating outside safe voltage level, monitor state of battery (State of Charge, State of Health), prompt/perform action when cell abnormalities occur (temperature, short-circuit), indicate end of life when capacity falls below set target threshold and perform cell balancing [9]. Almost all system which includes the usage of rechargeable batteries requires the use of BMS, without these place the battery may be damaged or catch fire.

There are many designs of BMS, they range from different target voltage requirements to amount of features they can have, some of these features include autonomous cell protection, cell balancing, can-bus communication (for vehicle applications) and daisy chaining for high voltage systems.

Each rechargeable battery has different chemistry which involves batteries being at a different voltage or operating threshold, caution must be taken into account when designing a BMS. For the case of lithium-ion cells, they exhibit non-linear charge/discharge curve, this can lead to difficulty in management, simply measuring voltage will not be sufficient, the BMS can execute complex algorithms which capture the SOC and SOH values of the cells.

## 1.2 Problem statement

Most wind turbine use similar systems to convert mechanical energy to electrical energy from the generators using either permanent magnet synchronous motor or induction motor, converters step up the voltage to match the grid. Variation of voltage and frequency in the converters are triggered by abnormal wind activity will cause the wind turbine to destabilise from the grid, this variation will also cause power losses in the cable which reduces the annual wind power output generation. Other alternatives which will discuss later have attempted to combat this issue but higher penetration of wind power can be achieved.

## 1.3 Aim

To design and integrate an small scale energy storage system (EES) using lithium-ion battery bank for an target commercial wind turbine with the aim of the design being cost effective when compared to ordinary wind turbine and to show benefits that the system brings to enable supply security.

## 1.4 Objectives

The EES wind turbine must act as a single unified system where power generated from the generator needs to be distributed to both the battery and the load. Monitoring, maintenance and protection of the

lithium-ion battery banks will be realised with the design of a BMS (battery management system) solution, for the prototype 3 to 5 lithium-ion cells will be used. The chosen 18650 cylindrical lithium-ion cell is one of the highest energy dense cell compared to any other battery technology today, they have an capacity of 100-256 Wh/kg [10]. The design of the BMS and the rechargeable battery bank must be targetted to an existing wind turbine, the Vestas V90 turbine will be looked at.

## 2 Literature Review

---

To understand the context of the project, we must investigate other similar systems that already exist.

### 2.1 Current approaches

#### 2.1.1 Microgrids

A Microgrid is a discrete energy system which comprises of electricity generation, energy storage and electrical load. These systems collect and store energy from renewable resources such as wind and solar and provides power to the consumers, they work like miniature power grid systems.

The energy storage within the microgrids enables minimal voltage and frequency deviations. Deviations of voltage and frequency occur due to sudden unexpected variations in renewable energy generation, this can cause power shortfall or excessive generation, the storage system acts as a buffer between the generator and the consumers to provide smoothing.

Microgrids is a solution to off grid power, they can either become connected to the grid to provide support during high demand of power or they can work independently off the grid this operation is called island mode. Island mode is an attractive feature, this provides areas which are disconnected from the grid (due to geographic position) to have power since the system is powered by renewable energy sources it will be self-sufficient.

The current system of micro-grids requires multitudes to work together to reduce the occurrence of destabilisation of the grid and supply emergency power in a case of a power outage. Generated wind energy must go through several stages of conversion before being stored in the micro-grid, they take the conventional path of converting the 3 phase ac to dc, dc to ac to match the grid then converted again from ac to dc to be accumulated in the microgrid energy storage [11].

#### 2.1.2 Academic Research

A published initial study paper by T.C Yang talks about the usage of rechargeable batteries in wind power generation with variable speed induction generators [3]. He discusses that external energy storage plants have already existed to combat challenges caused by intermittency of renewable power generation, the cost of using EES based system compared to 'external' plants will lower the costs.

The addition of the EES system within the turbine can integrate with existing AC to DC and DC to AC converters. For the following case study shows that in a wind farm of 50 wind turbine can be replaced with 10 wind turbines with EES in each of them plus 33 ordinary ones which would produce an equal amount of annual wind energy output.

If you mention [12], you do not have to mention the title of the paper

Looking at another published paper "Battery Energy StorageSystem (BESS) and Battery Management System (BMS) for Grid-Scale Applications" [12], source suggests that we produce more power than necessary to ensure adequate power quality, in-efficiencies like these can be removed by using energy storage such as lithium-ion cells and vanadium redox-flow batteries. BESS requires a battery management system which can monitor and provide safe, optimal operation for every battery pack and can be linked with a system supervisory control (SSC) to monitor the full system. BESS brings along few key advantages to the grid they include: matching peak power demand, load following to increase generation utilization, improve grid stability, power quality and frequency balancing.

In recent years, energy storage prices (\$/KWh)

Energy storage costs in the past had higher cost, it was more economical to build more power generation facilities than it was to store. ~~As of recent years prices of energy storage prices~~ continue to fall while there recharge cycle increases, current technologies are able to provide better understanding and quantitative predictive modelling approach for improved cycle life. The computing power nowadays can facilitate more

processing power, it is possible to have advance BMS with better SOC and SOH approximation based algorithms. With BESS, the phase of voltage and current on grid can be matched to provide a near unity power factor greater than 99% with the THD less than 5% and each corresponding harmonic components less than 3%.

### 2.1.3 Line-Interactive UPS

Uninterruptible power supply is a collection of energy storage which provide emergency power to the load when main power generation fails, there are two types of UPS, offline UPS and line interactive UPS. Line interactive UPS have a addition of built in Automatic Voltage Stabilizer (AVS), this ensures that the voltage remains within pre-defined voltage windows.

Figure 1 shows how the line-interactive UPS systems are connected, an article source [1] suggests these UPS have two modes of operation stand-alone and grid connected mode, to connect to the grid power flow is controlled using frequency and voltage drooping techniques.

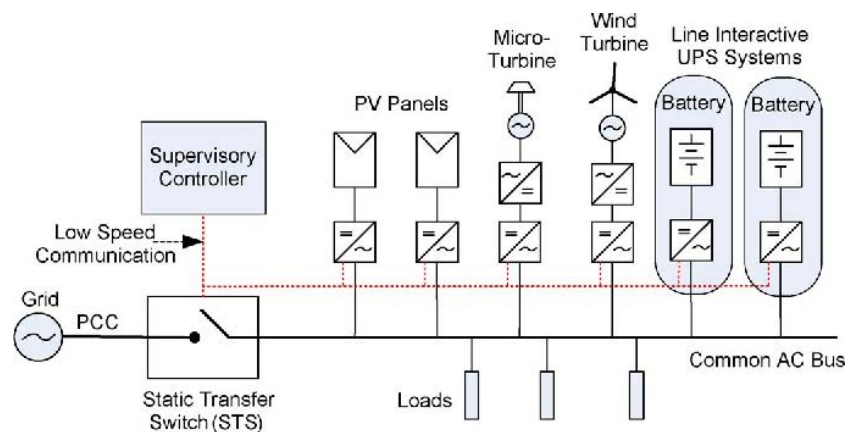
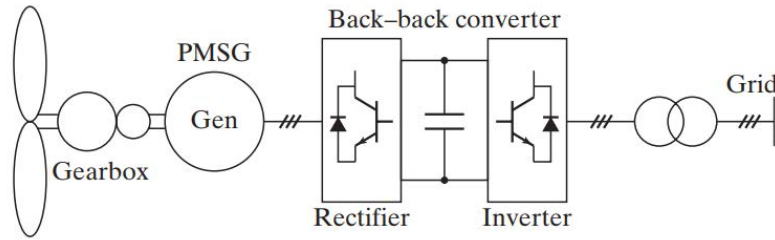


Figure 1: Grid Structure [1]

### 3 Simulink Modelling

#### 3.1 Proposed Model Design

An PMSG variable speed wind turbine is an simple and low cost design which commonly used in many wind farms, the excitation of the PMSG is fixed and can exhibit high power density characteristic. Figure 2 illustrates a model of an typical PMSG wind turbine, it contains an fully controllable PWM controlled converter which is used to obtain maximum efficiency from intermittent wind. For our proposed design we will fully simulate this simple model with addition of an BESS, this can be seen in figure 3.



If this image from somewhere else, it must be referenced

Figure 2: Typical model of PMSG wind turbines

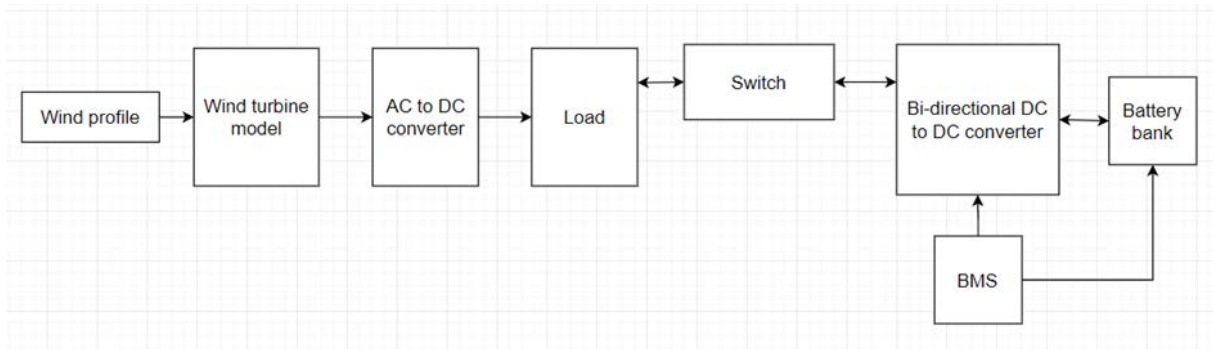


Figure 3: Proposed Simulation Model Structure

#### 3.2 Wind Turbine Model

##### 3.2.1 Theoretical Approximation & Considerations Either use Equation (1) or Eq. (1)

Equation (1) shows the maximum theoretical power output of an wind turbine, the wind speed entering the turbine is higher than leaving the turbine and the power is to the cubic power of wind velocity. It is stated that the maximum achievable extraction of wind power is at best  $\approx 59\%$  of the total kinetic energy of air flowing through wind turbine. The equation has parameters:  $\rho$  is the air density,  $A$  is the area swept by the blades,  $C_p$  is the power co-efficient and  $v$  is the velocity.

$$P_t = 0.5\rho AC_p(\lambda, \beta)v^3 \quad (1)$$

Given an example we will attempt to provide an calculative approach then view the power output in simulation, if we had the elevation to be of wind turbine to be 90m, each blade is 22m, the average air temperature

to be 30°C and the wind speed to be 10m/s, then:

$$\text{Air Density} = \delta = \frac{353}{T + 273} e^{\frac{-h}{29.3*(T+273)}} = 1.172 \text{kg/m}^3 \quad (2)$$

$$\text{Wind Density} = \rho = \frac{P_{in}}{A_s} = 586.2 \text{W/m}^3 \quad (3)$$

$$\text{Area Swept by blades} = A_s = \pi r^2 = 1520 \text{m}^2 \quad (4)$$

$$\text{Power in wind} = P_{wind} = \rho A_s = 891 \text{kW} \quad (5)$$

Power curve of a wind turbine relates the mechanical power to the wind speed, this defines the power characteristics. Figure 4 shows an graph divided into 3 quadrants: cut-in, normal operating and cut-out. With reference to Vestas V90[6] wind turbine specification in cut-in this is the minimum required wind speed to start the turbine which is 4m/s, in normal operating range the wind turbine can supply power which has a cubic relation with wind speed and finally at cut-out wind speed is where the wind turbine goes beyond rated power and will stop rotating to prevent potential damage as the rotor may spin to quickly.

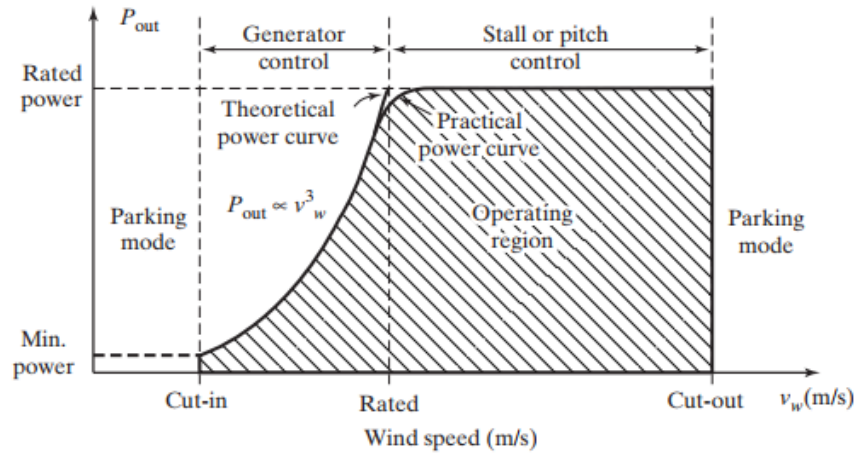


Figure 4: Wind Turbine Generic Power Curve

### 3.2.2 Simulation Model

Figure 5(a) shows two wind profile inputs fed into the existing PSMG wind turbine model[13], a step model is used to test the behaviour under sharp changing wind speeds and the other profile is based off a real time varying wind sample. Varying wind speed is fed into wind turbine model block which takes three parameters: generator speed, wind speed and pitch angle, the output of this computation produces torque which is fed to the PSMG block. The output of the wind turbine model is an 3 phase voltage which is rectified to a DC voltage for next stage, figure 5(b) shows the workings of the PSMG model, this model

does not contain MPPT block but does include other blocks such as pitch control and torque computation. The results of simulation will be discussed in the later sections.

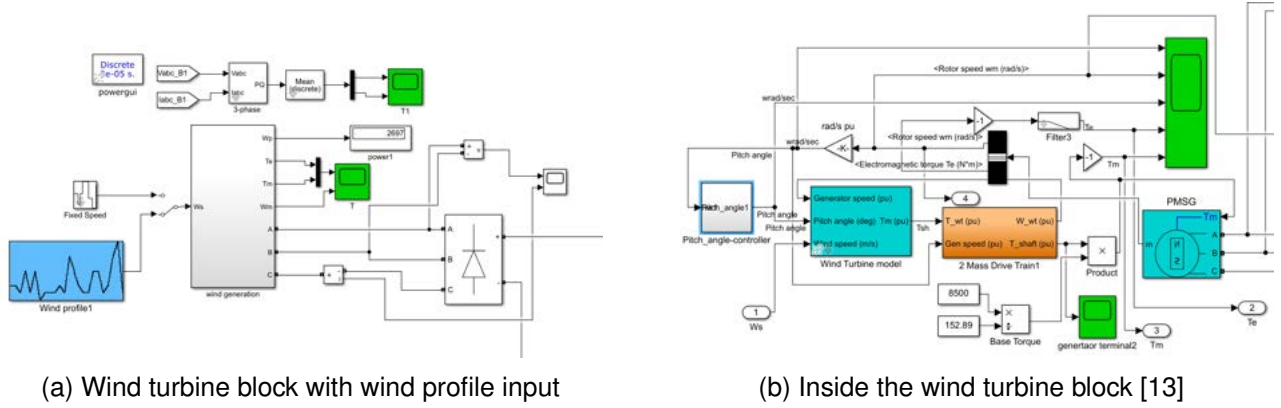


Figure 5: Wind turbine simulation model

Can the above images be bigger?

| PARAMETER                    | VALUE          |
|------------------------------|----------------|
| <b>Wind Turbine Model</b>    |                |
| Power Co-efficient ( $C_p$ ) | 0.5            |
| Area swept ( $A$ )           | 1520 $m^2$     |
| Wind velocity ( $v$ )        | Variable       |
| Air density ( $\rho$ )       | 586.2 $W/m^3$  |
| Base torque ( $T_m$ )        | 56Nm           |
| <b>PSMG Configuration</b>    |                |
| Number of phase              | 3              |
| Flux linkage                 | 0.433 Wb-t     |
| Stator phase resistance      | 0.425 $\Omega$ |
| Stator inductance            | 0.0082 H       |

Table 1: PSMG Wind Turbine Model Simulation Parameters

### 3.3 Bi-directional Converter Design

To connect the battery bank to the system there needs to be an intermediate stage which can regulate the flow of power in both directions, we design bi-directional DC-DC converter which allows for charging (buck mode) and discharging (boost mode) of the battery bank. A bi-directional converter must be designed to meet the specification to ensure correct operation (i.e correct charging voltage) and work within acceptable tolerances. Table 2 & 3 shows the values of important parameters, calculations carried out to find the required duty cycle, capacitance and inductor values[14] for the converter.

### 3.3.1 Specifications

| PARAMETERS                 | FORMULA/TYPE   | CALCULATED VALUES |
|----------------------------|--|-------------------|
| Input Voltage (V)          | Variable   | 530V              |
| Average Output Voltage (V) | Variable   | 480V              |
| Ripple Voltage (V)         | Variable   | 10V               |
| Ripple Current (I)         | Variable   | 5A                |
| Switching Frequency        | Variable   | 10000 Hz          |
| Duty cycle (k)             | $\frac{V_{\text{Average output}}}{V_{\text{input}}}$ | 69.57%            |
| Inductance (L)             | $\frac{V_{\text{input}} k(1 - k)}{f \Delta I}$       | 2.92mH            |
| Capacitance (C)            | $\frac{V_{\text{input}} k(1 - k)}{8LC f^2}$          | 6.25uF            |

Table 2: Buck Converter Calculations



| PARAMETERS                 | FORMULA/TYPE   | CALCULATED VALUES |
|----------------------------|--|-------------------|
| Input Voltage (V)          | Variable   | 480V              |
| Average Output Voltage (V) | Variable   | 550V              |
| Ripple Voltage (V)         | Variable   | 5V                |
| Average Current (I)        | Variable   | 50A               |
| Ripple Current (I)         | Variable   | 5A                |
| Switching Frequency        | Variable   | 10000 Hz          |
| Duty cycle (k)             | $1 - \frac{V_{\text{input}}}{V_{\text{Average output}}}$ | 12.73%            |
| Inductance (L)             | $\frac{V_{\text{input}} k}{f \Delta I}$                  | 1.22mH            |
| Capacitance (C)            | $\frac{I_{\text{Average}} k}{f \Delta V}$                | 0.127mF           |

Table 3: Boost Converter Calculations

### 3.3.2 Model

The bi-directional converter composes of two major sub parts: the active elements and the control logic. In our design we have specified for the control logic to switch from buck mode (charging) to boost mode (discharging) when the voltage generated from the wind turbine drops below 480V, this is to stabilise the voltage dip. The control logic in this model is an open-loop system with fixed duty cycle for testing, an closed loop feedback control system with the help of an micro-controller will be discussed in the later sections. With reference to table 3 the parameter ripple voltage is made set to be approximately 5V, this is to set to smooth the peak to peak voltage, another consideration we made is the switching frequency is made to be high in order to achieve greater converter efficiency.

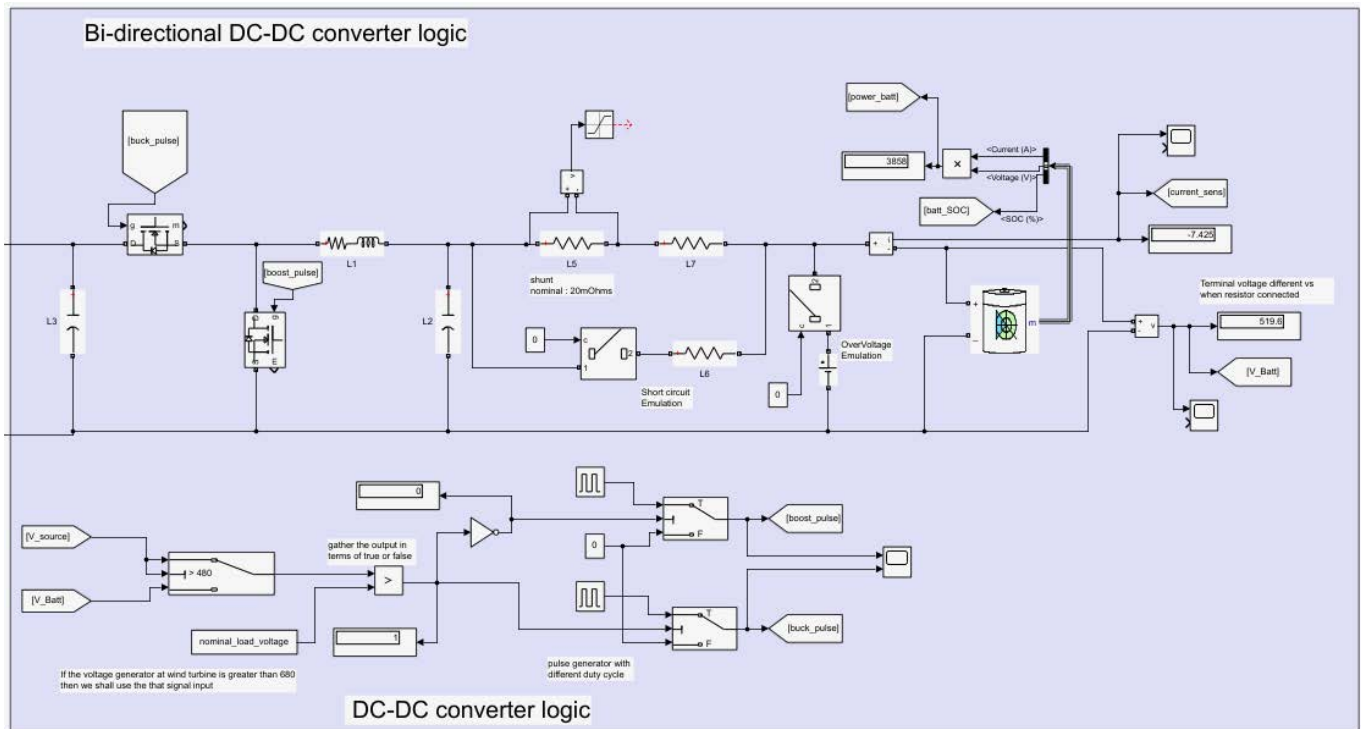


Figure 6: Bi-directional Converter Model

In what software the model above is developed? Matlab/Simulink? please mention

### 3.4 Battery Model and Choice

For our simulation we used an generic lithium ion battery model, correct parameters are added to this model to present out target cell, figure 7 indicate outcome of setting the parameters according to the data-sheet.

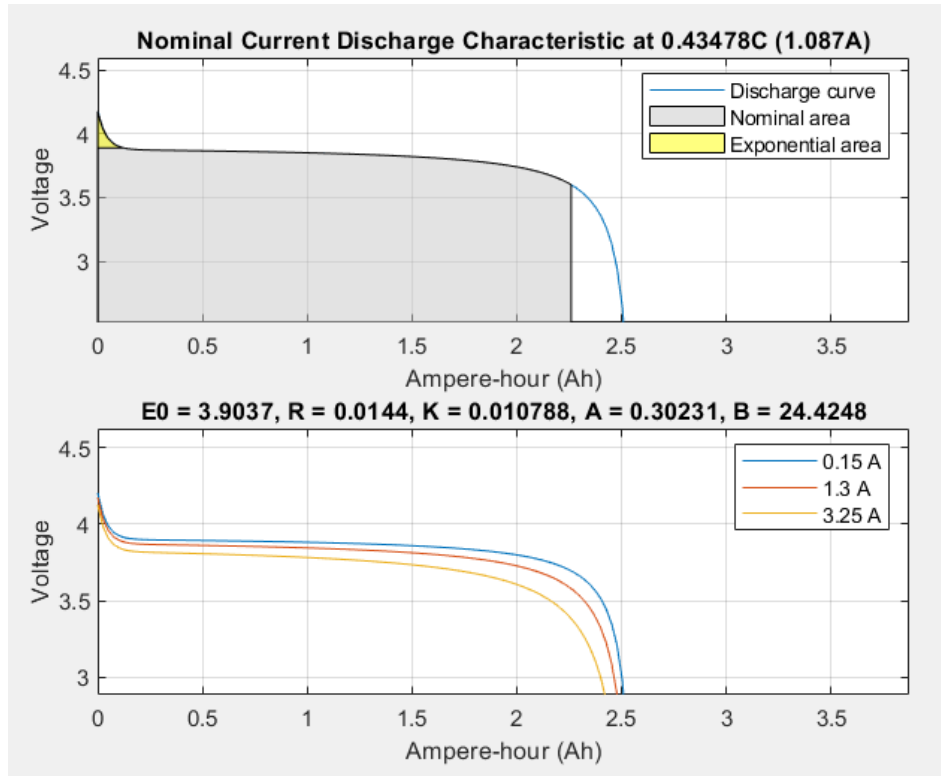


Figure 7: Single Lithium ion model plot with Simulink

The capacity of our battery bank needs to be known for our simulation model, a single battery bank in the design is specified to carry a capacity of 100KWh. From the datasheet for the Samsung INR18650 the rated capacity is 2500mAh, we compute that:

$$\text{Wh of single cell} = \frac{\text{mAh of single cell} * \text{Nominal voltage of the cell}}{1000} = 9.25Wh \quad (6)$$

Next we determine the number of cells required for an 100KWh battery bank:

$$\text{Total amount of cells required} = \frac{\text{Target capacity of battery bank}}{\text{Wh of single cell}} = 10810 \quad (7)$$

We calculate the number of cells required in series for an nominal target voltage of 480V:

$$\text{No. of cells required in series} = \frac{\text{Nominal target voltage of battery bank}}{\text{Nominal operating voltage of cell}} = 130 \quad (8)$$

Finally, to determine the amount of cells in a parallel configuration is:

$$\text{No. of cells required in parallel} = \frac{\text{Total amount of cells required}}{\text{No. of cells required in series}} = 84 \quad (9)$$

From our calculations we find the configuration for our battery bank to have 130s84p. The choice of battery bank size and nominal charging voltage is important as they impact the discharge cycles of the cells, a high nominal charging voltage can reduce the discharge cycles, source [15] states that with a charge level of 4.2V we get  $\approx 400$  cycles whereas with a voltage of 3.9V we get an  $\approx 3000$  cycles.

## 4 3D Modelling

---

### 4.1 Model Motivation

To know realistically if a battery bank can fit within the wind turbine we have to have a medium to visualize the 3D model. The first step to take is to view the wind turbine of interest we opted to use an existing model of an Vesta V90 2MW wind turbine[16], this model gave a good sense of size to work with. Advantages of developing a model:

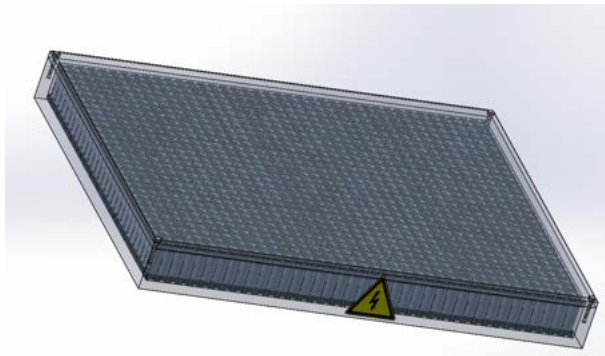
1. Easily update model if a new design change arises
2. Bill of material provides an estimated cost for the components used in the model, thus lowering risk of cost uncertainty
3. Combine pre-existing model with a new custom model to quickly come up with an solution for approvals
4. 3D model can show accurate measurements and proportions of an object
5. Fewer instructions and no language barriers

### 4.2 Software package

Solidworks is <sup>a</sup>~~an~~ solid modelling computer-aided design software which we used to design the model, this package provides many features which aid design workflow and improve project approvals, they include: large assembly design to visualize over 3000 components, detailed drawing blueprints, photo-realistic renders, revealing through exploded view what makes up a object and air flow simulation to view temperature environment.

### 4.3 Justification

Within the wind turbine it is known to be hollow and there is vast amount of space to work with, we start from ground up to produce the battery bank by looking at the dimensions of an Samsung lithium ion cell[17]. We roughly know the approximate amount of cells required in total based off our specifications this helps us to know how much space will be taken up within the wind turbine, figure 8(a) shows a custom made battery pack. The arrangement of the cells in the battery pack is by no means optimal or efficient, some designs out there employ the use of honeycomb arrangement due to the cylindrical nature of the cells. Figure 8(b) illustrates an custom made battery bank which holds multiple battery packs, an battery bank designed in this model has an capacity of 100kWh, ideally each battery pack will contain an BMS module.



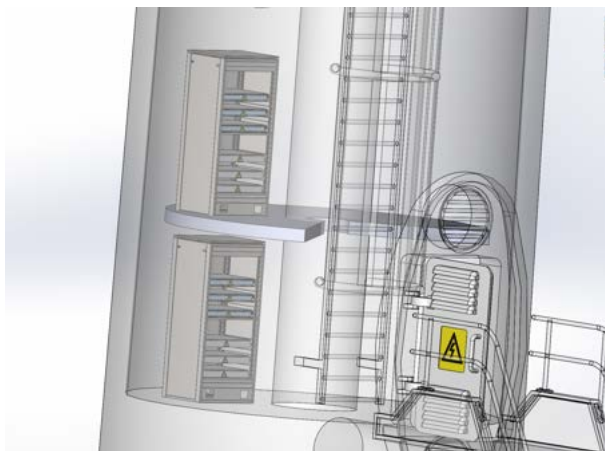
(a) Battery Pack



(b) Battery Bank

Figure 8: Model of Battery Housing

Figure 9(a) shows the battery bank placed within the model wind turbine, the height of the battery bank is  $\approx 2\text{m}$  whereas the hub height of the wind turbine is  $\approx 90\text{m}$ . If each battery bank is  $100\text{kWh}$  then on a single platform there will not be enough room to place more than 2, we can see the addition of an platform which can be used to place more. We use the cut-away feature in Solidworks to slice open a portion of the wind turbine and realistic photo rendering to view the model, and in figure 10 we can see the full render, this model is made to be at the correct proportion.



(a) Wireframe View



(b) Realistic Rendered View

Figure 9: Housing the Battery Bank within Wind Turbine



Figure 10: Render of Full Turbine

## 5 Battery Management System Design

### 5.1 Technical Background

A battery management system is an electronic device which provides protect battery from operating outside safe voltage level, monitor state of battery (State of Charge, State of Health), prompt/perform action when cell abnormalities occur (temperature, short-circuit), indicate end of life when capacity falls below set target threshold and perform cell balancing [9]. For the case of lithium-ion cells, they exhibit non-linear charge/discharge curve, this can lead to difficulty in management.

The complexity of the BMS depends on the individual application, for our approach on the custom BMS we look into an embedded solution which involves both hardware and software technicalities, the goal is to have a good balance of safety and reliability. With well defined software we can have greater control over the operation to ensure that the battery storage is always online for every instance the wind turbine begins to desynchronise and we can employ intelligent algorithms for example, detect faulty sensors, thus increasing safety.

#### 5.1.1 BQ76920 Analogue Front End Chip

Analog front end devices serves as part of complete pack monitoring and protection solutions for next-generation high power systems, it directly interfaces with the cells it is monitoring, the BQ76920 is chosen as it has the capabilities in supporting critical devices such as uninterruptible power supplies. The BQ76920 AFE uses a pure digital interface to provide the host controller (main micro-controller) information on the cells through I2C communication, we can control the AFE using the host controller by sending commands.

Table 4 lists the comparisons of BMS ICs mentioned, these values were taken from their datasheet. We compared a few parameters which determines the choice of AFE, we can see that that the BQ76920 has one of the highest voltage precision accuracy with the lowest measurement down to 0.75mV and the development time to produce the first prototype is not too high.

| MANUFACTURER NAME |              |            | DEVELOPMENT TIME | VOLTAGE AC-CURACY (mV) | COMMS      | COST CHIP | PER |
|-------------------|--------------|------------|------------------|------------------------|------------|-----------|-----|
| Texas Instruments | Instru-ments | BQ76920    | Medium           | 0.75                   | YES - I2C  | 2.00      |     |
| Texas Instruments | Instru-ments | bq76PL4551 | High             | 0.75                   | YES - UART | 2.50      |     |
| Linear Technology | Technol-ogy  | LTC6802-1  | Low              | 35                     | NONE       | 0.97      |     |
| Analog Devices    |              | AD7280     | Medium           | 10                     | YES - SPI  | 1.00      |     |

Table 4: Boost Converter Calculations

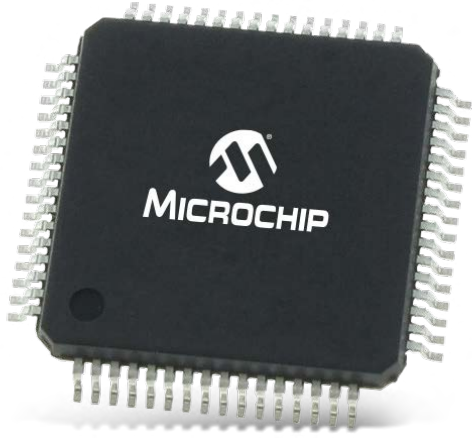
#### 5.1.2 PIC16F1719 Micro-controller

The choice of micro-controller will play a big factor in the development time, it is important that the micro-controller chosen can meet our specifications. We take note on the peripherals onboard, peripherals are devices within the micro-controller which provide interfaces with the outside world, some examples general purpose input IO, I2C, analog to digital converters and timers.

There are many distributors and flavors of micro-controllers, we have manufacturers from Atmel, Arm cor-



tex, Motorola and PIC. We use the PIC16F1719 is an 8-bit micro in our design as the host controller, with large program memory of 16384 bytes, 2048 bytes of RAM and large variety of peripherals makes it suitable. For development time, PIC has a great database resource to provide knowledge of programming and it is backed by a strong community base. Another reason for choice is the ability to debug which is a essential tool for viewing the behaviour of complex software, we use the PICKIT 3 which is an powerful debugger tool that connects to the micro-controller, this can be seen in figure 11(b).



(a) Surface mount chip

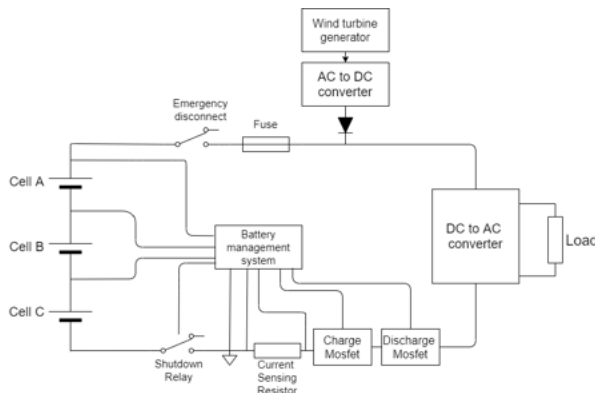


(b) Programmer for the micro-controller

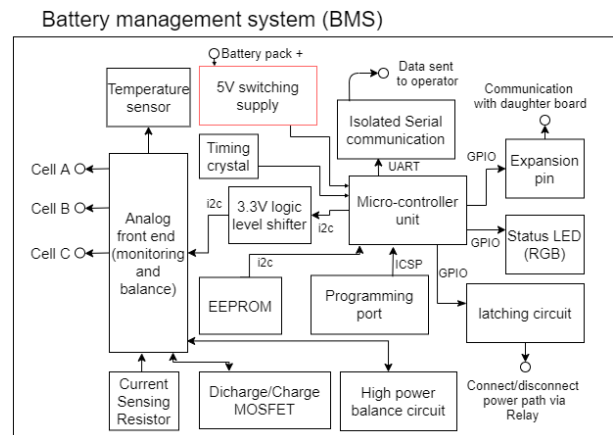
Figure 11: Microchip products

## 5.2 Overview & Specification

### 5.2.1 System Block Diagram



(a) System block diagram



(b) BMS Block Diagram

Figure 12: Block Diagram of system

Can the above diagrams be bigger?

### 5.2.2 Functionality & Features

Table 5 lists all the features which will be programmed into the BMS, the basic features are the bare minimum of what an BMS should include to function, we enhance our design by bringing more unique features to improve the safety and longevity of the cells. These features are designed around our proposed specification demonstrated by the modelled in our simulation, the working principle of the features will be described in the next few sub sections.

| BASIC  | UNIQUE   |
|--|--|
| Pack over-current in discharge                       | State machine with low latency interrupt to protect battery bank as fast as possible   |
| Pack short circuit in discharge                      | Precise temperature measurement technique using Steinhart & Hart equations   |
| Cell under-voltage protection                        | Battery unloading and periodic SOC measuring via lookup table in EEPROM to re-calibrate estimated SOC  |
| Cell over-voltage protection                         | Watchdog timer to prevent communication lockup with BQ76920 analog front end chip  |
| Coloumb Counting                                     | Reporting status and battery information over isolated communication channel   |
| Monitoring individual cell voltages                  | PI controller to adjust charging voltage provided by bi-directional converter, PWM type control signal based on pack current and temperature |
| Choice of low/high power cell balancing (50mA/150mA) |  |

Table 5: BMS Features

### 5.3 Pin Definitions

| PIN NO. | FUNCTION |
|---------|----------|
| 1       |          |
| 2       |          |
| 3       |          |
| 4       |          |
| 5       |          |
| 6       |          |
| 7       |          |

Table 6: Pin definition for PIC16F1719

No function is allocated to the pins, is this going to be completed in the final report?

## 5.4 Software

### 5.4.1 Flow Chart

The text within the boxes are hardly readable.  
Make the font size bigger

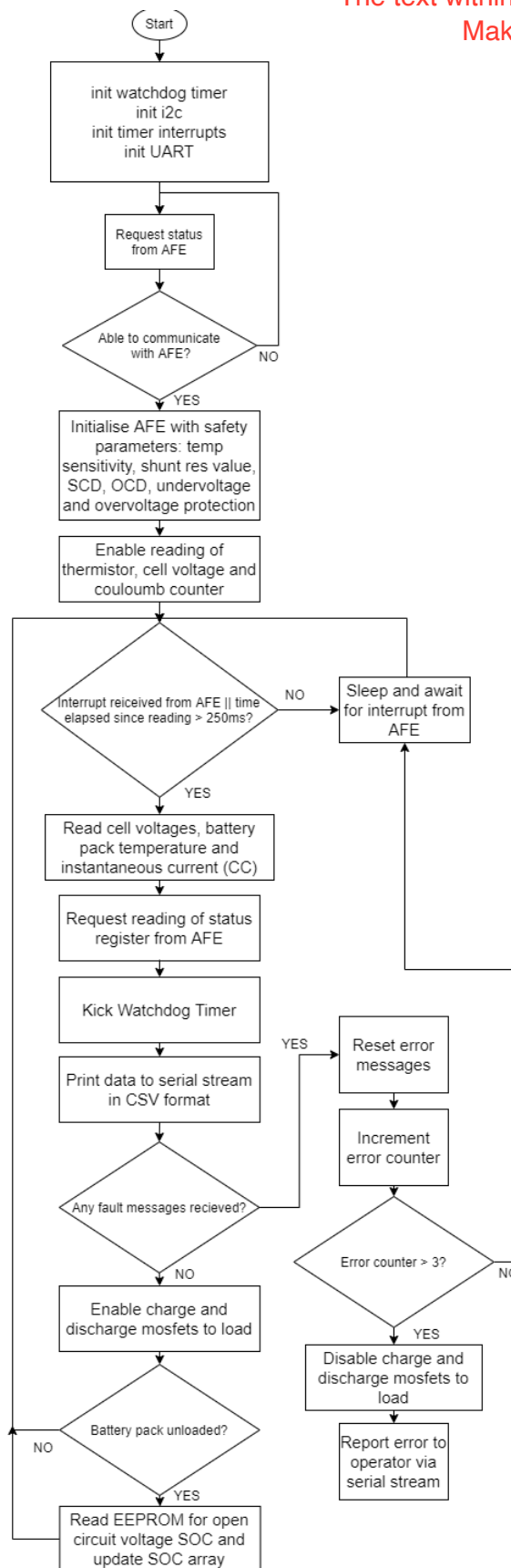


Figure 13: Flowchart of Firmware

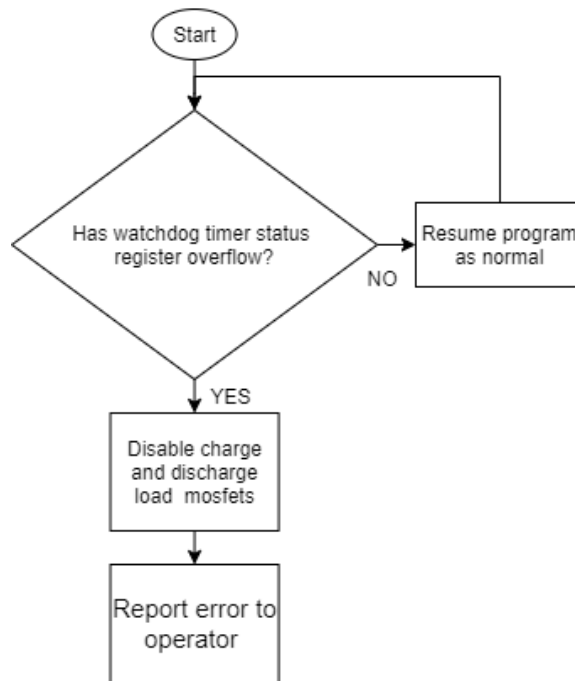


Figure 14: Watchdog Timer Parallel process

## 5.4.2 Algorithms and Software Design

### 5.4.2.1 Finite State Machine

We use a state machine model with limited number of states to determine what status the BMS should be in, defining a finite amount of known states means that our BMS will be deterministic. State machine model design provides key advantages such as lower processor overhead, convert design abstraction to code execution and flexibility. For our BMS, we defined 4 states: Await AFE connection, AFE initialization, Read AFE parameters and AFE error states.

### 5.4.2.2 Communications with connected devices on bus using I2C protocol

I2C is an synchronous master-slave packet-switched simplex serial protocol where multiple devices can be connected to one bus, it requires two wires from the device which includes SCL (clock synchronization signal) and SDA (data signal), this is a commonly used peripheral. In our BMS the main micro-controller PIC16F1719 is the master device talking to two other slave devices on the I2C bus the BQ76920 AFE and the EEPROM chips, each device has their own unique identification code and listens on the bus to await for command. Figure 15 shows how the devices are connected together on the bus, based on our specification we opted to use I2C communication as the speed of this protocol is sufficient at bit rate of 100KHz.

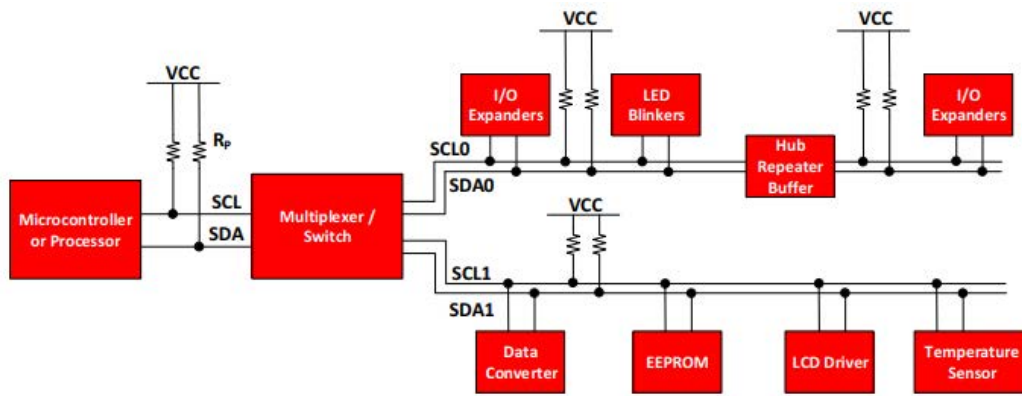


Figure 15: I2C Communication example cited from TI[2]

The text within the boxes are hardly readable.

Make the font size bigger

I2C is the backbone for communication between devices as it can relay important battery parameters to the master device. With reference to our flowchart in figure 13, we start by initialising basic protection parameters such as current to trip over-current, precision of cell voltage measurement to the AFE by producing static pre-defined setting in the micro-controller and sending this over I2C bus to the AFE chip, we use the documentation provided by Texas instrument[2] to create an function for writing over I2C (figure 16).

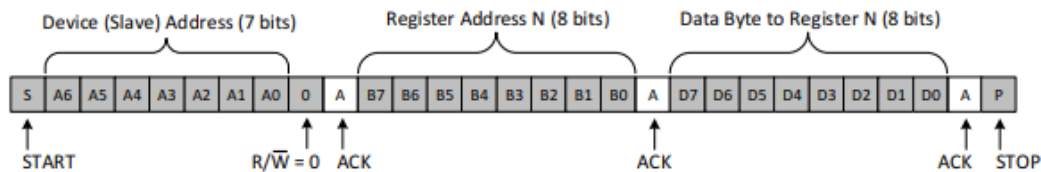


Figure 16: I2C Communication write byte stream

```

1 void I2C_writeRegister(int slaveAddress, int regAddress, int data) {
2   send_I2C_startBit();
3   send_I2C_controlByte(slaveAddress, WRITE);
4   send_I2C_data(regAddress); //write to the reg address of slave
5   send_I2C_data(data);
6   send_I2C_stopBit();
7 }

```

Listing 1: Function to write data to slave device using I2C

### 5.4.2.3 Watchdog Timer

The watchdog timer is an peripheral within the PIC16F1719 micro-controller which acts as an specialized timer module which monitors if an function takes an extended amount of time to execute, this runs in the background parallel to running code. We employ the watchdog timer to continuously monitor the i2c communication between the AFE and the micro-controller, in the code, we expect a communication every 250ms if there is no communication for more than a duration of upper threshold of 300ms the micro-controller should carry out methods to react to this change, in list below we move to the error state and shut down the BMS to prevent any potential damage.

```

1 void watchdog_timeout_shutdown() {
2   //check if watchdog timer expired
3   if (!STATUSbits.nTO) {
4     RGB_color(RGB_RED);

```

```

5  __delay_ms(2000); //allow time to signal error to operator
6  currState = AFE.COMM.ERROR; //change to error state
7  Shutdown_BMS(); //call function to disconnect the battery pack
8  }
9  }

```

Listing 2: Wtachdog - Function to shutdown

#### 5.4.2.4 SOC estimation and correction

Grid connected battery systems are usually large and expensive, therefore even a small improvement in utilisation can lead to great economical savings. The result of these improvements can be made within the algorithm and control scheme. A basic BMS controls the battery pack to only meet the power demand, a intelligent based BMS with control algorithms can reduce the degradation of cells and this system is especially important for large battery pack[12].

During charging cycle it is important to gauge SOC of each battery bank especially for constant current charging schemes, as inaccurate SOC can lead to under/overcharging. BMS is required to charge/discharges battery bank to correct SOC for optimal cell life and performance, it may not be necessary to always keep the cells topped up at 100% SOC, infact this can be detrimental to cell health in the long run.

There are several techniques employed to find SOC in an cell, the best technique would be to use open circuit voltage (OCV) measurement where their is no load on the cell and the voltage is taken at the terminal at steady state. The reading is then used to compare to an cell discharge curve to pinpoint SOC, unfortunately this technique is not pratical some disadvantages associated with it include long measurement time and the fact that the cell must be completely disconnected from the system. We can still use this method to determine the accuracy of other SOC approximation techniques.

Colorimetric counting most common and pratical technique used to estimate SOC, integration of current with respect to time to get the C/Ah which is converted to find SOC, this type of measurement scheme will be used within our algorithms. The equation (10) uses  $Q_r$  - the amount of charge present in battery,  $Q_c$  - the full capacity of battery and  $I$  - the current which can be either negative or positive[18]. Equation (10) cannot be fully implemented into the micro-controller as it in continuous form, for a digital interface we have to take the discrete computation of SOC by taking samples every interval.

$$\text{SoC}(\%) = \frac{Q_r \pm \int I dt}{Q_c} * 100 \quad (10)$$

In the case where battery bank SOC is optimal and there is no de-synchronization occurrence, we use 24lc256 EEPROM chip to enhance the SOC approximation by storing the OCV lookup table for the Samsung INR18650 lithium-ion cell where the OCV value can be read by the host micro-controller to update the SOC values for all cells, this can correct SOC offset/errors from colorimetric counting algorithm. Figure 17 shows the plot of a size of 50 samples for the OCV measurements, the accuracy for SOC can be improved if we increase the stored sample values, this is especially important for improve the resolution of the curve points in the figure, the downside of increasing the amount of stored sampled values is the access times can increase. The 24lc256 EEPROM chip has benefits of 32Kbytes storage, an data retention of 200 years and access time of 900ns which is sufficient for our requirements.

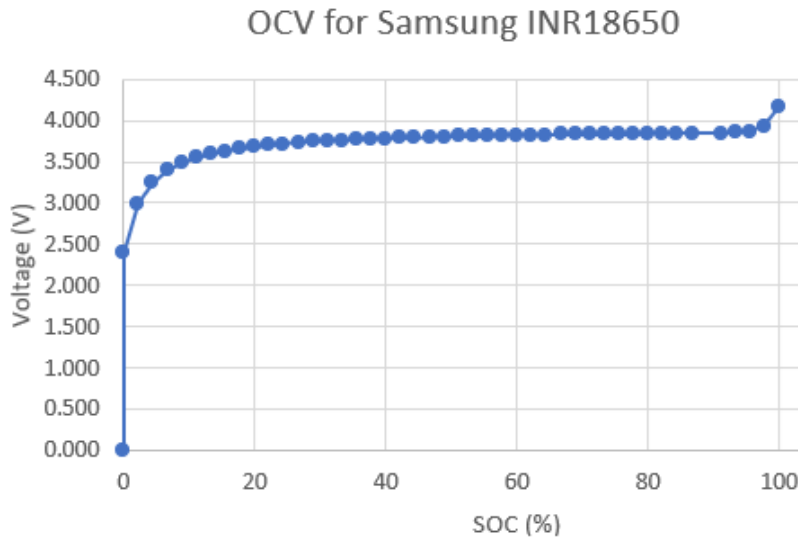


Figure 17: OCV Graph

#### 5.4.2.5 NTC thermistor using Stein-hart and Hart approach

##### Introduction

Knowing the accurate and precise temperature value of the battery pack will enable our system to quickly react to these changes. The temperature specification of the Samsung cell given in the datasheet informs a tight constraint of maximum rated cell temperature of 60°C, the implication of operating at such temperature for a prolonged period of time will degrade the cell thus requiring frequent replacement. There is optimum temperatures condition for charging and discharging of the cell which we will need to consider. In our battery pack design it is important to distribute multiple temperature sensing units through out the pack to improve localisation, this will help us find a better average temperature of the whole pack.

The negative temperature co-efficient (NTC) thermistor is an temperature dependant resistor, we opt to choose this sensor over the positive temperature co-efficient (PTC) thermistor as this element includes an amplification op-amp to operate which degrade signal to noise ratio. NTC thermistor have no other element within aside from the sensing transducer and general cost is cheaper.

Temperature measurement not need to be precise as the OCV SOC for the use of lookup table, producing a lookup table takes a significant amount of time and memory from the micro-controller. Specified in the thermistor data sheet are the resistance tolerances when the part is manufactured, to reduce uncertainty measurement of the thermistor resistance at few temperature points will be noted, we can then use mathematical approximation methods to plot the characteristic curve for the thermistor.

##### Approximation Model

NTC thermistor are non-linear resistors there are several approximation methods available to define its characteristic, one of the basic technique involves calculating the  $\beta$  co-efficient, this co-efficient simply describes the non-linear curve and requires two known variables of temperature and resistance to compute shown from eq.(11).

$$\beta = \frac{\ln \frac{R_{T1}}{R_{T2}}}{\left(\frac{1}{T_1} - \frac{1}{T_2}\right)} \quad (11)$$

The Stein-hart & Hart approximation model which we will adopt is more accurate than  $\beta$  model, this requires three samples of temperature and resistances over a given range to form three thermistor constants shown in general eq.(12). Three simultaneous equations are formed and shown as a matrix(13), we use matlab to solve using the inverse matrices law to find co-efficient(14).

$$\frac{1}{T + 273.15} = A + B \ln(R_T) + C \ln(R_T)^3 \quad (12)$$

$$\begin{bmatrix} 1 & \ln(R_{T1}) & \ln(R_{T1})^3 \\ 1 & \ln(R_{T2}) & \ln(R_{T2})^3 \\ 1 & \ln(R_{T3}) & \ln(R_{T3})^3 \end{bmatrix} \begin{bmatrix} A \\ B \\ C \end{bmatrix} = \begin{bmatrix} \frac{1}{T1+273.15} \\ \frac{1}{T2+273.15} \\ \frac{1}{T3+273.15} \end{bmatrix} \quad (13)$$

$$\begin{aligned} AX &= B \\ A^{-1}AX &= A^{-1}B \\ X &= A^{-1}B \end{aligned} \quad (14)$$

Re-arranging the variable T in eq.(12) we can find the temperature at a specified resistance the equation will be programmed into the micro-controller to carry out the execution, too visualise our characteristic curve we plot a graph shown in Figure 18 based oon our sampled data and co-efficient from Table 7.

| MEASURED/CALCULATED PARAMETER     | VALUE                |
|-----------------------------------|----------------------|
| Temperature & Resistance sample 1 | 18C & 12000 $\Omega$ |
| Temperature & Resistance sample 2 | 25C & 10000 $\Omega$ |
| Temperature & Resistance sample 3 | 30C & 9000 $\Omega$  |
| Steinhart co-efficient A          | -0.017428133935807   |
| Steinhart co-efficient B          | 0.003137120345556    |
| Steinhart co-efficient C          | -0.000010382213834   |

Table 7: Recorded parameters of RS PRO NTC thermistor



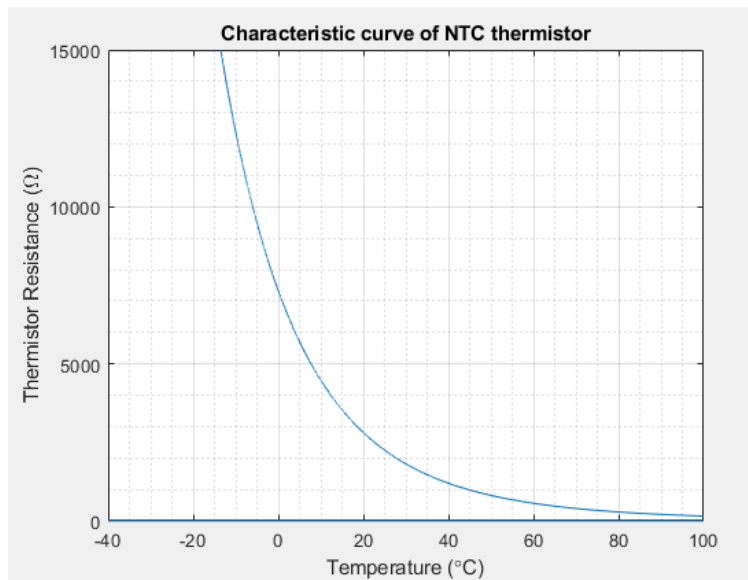


Figure 18: NTC thermistor curve

## Code implementation

```

1  /*
2  @brief: function to read the temperature on battery pack according to 10k NTC thermistor
        datasheet
3  */
4  void updateTemperatures() {
5      float tmp = 0;
6      int adcVal = 0;
7      int vtsx = 0;
8      unsigned long rts = 0;
9      adcVal = ((readRegister(AFE_BQ76920_I2C_ADDRESS, TS1_HI_BYTE) & 0x3F) << 8) | readRegister(
        AFE_BQ76920_I2C_ADDRESS, TS1_LO_BYTE);
10     vtsx = adcVal * 0.382; // mV
11     rts = 10000.0 * vtsx / (3300.0 - vtsx); // Ohm
12     //co-efficient a,b,c
13     tmp = 1 / (-0.017428133935807 + 0.003137120345556*log(rts) + -0.000010382213834 *(log(rts)*log(
        rts)*log(rts))); // K
14     temperatureThermistor = (tmp - 273.15)*100;
15 }

```

Listing 3: Function to compute temperature of battery pack

### 5.4.2.6 Isolated Serial Communication

we make the communication channel for sending information to operator galvanically isolated this required to protect low voltage circuitry against high voltage systems. Another communication peripheral of the PIC16F1719 micro-controller we use is the UART, we demonstrate in the testing phase which is discussed later in the section how we read the CSV information from the BMS to view how our BMS performs.

CSV Format:

Battery Pack Voltage, Pack Current, Temperature reading, Cell V1, Cell V2, Cell V3, Cell V4, Cell V5, SOC Cell 1, SOC Cell 2, SOC Cell 3, SOC Cell 4, SOC Cell 5, XR Error, Alert Error, Undervoltage Error, Overvoltage Error, Short circuit discharge Error, Overcurrent discharge Error

## 5.5 Hardware

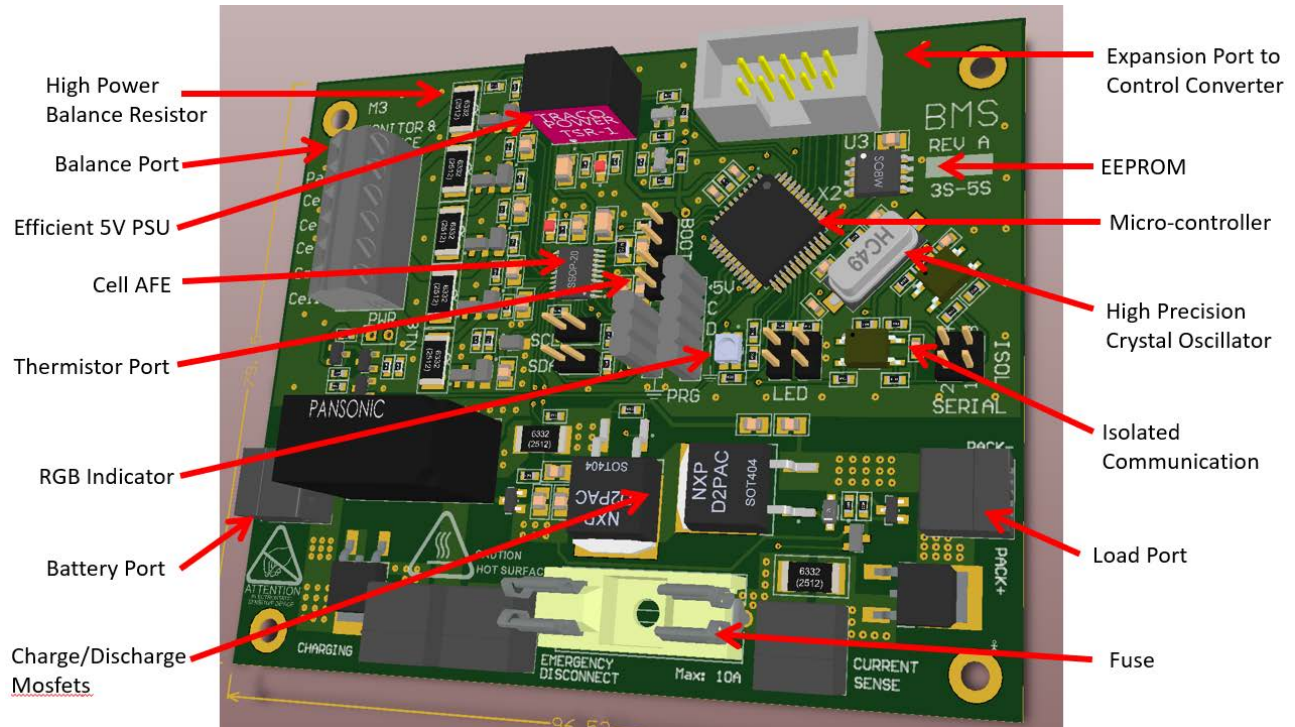


Figure 19: Components of the BMS Hardware

### 5.5.1 PCB Design

PCB is the final stage of pre-circuit testing, this process combines the component placement and routing. A PCB is designed to fit all the components on our schematic in an efficient and compact manner, realising this circuit on a breadboard would be difficult due to size, we can perform circuit testing for analog sub-circuits which work independently from the micro-controller. Using the PCB design package tool we can realise some benefits: we are able to find out the measurement of the board to fit into our enclosure, figure 19 shows an 3D model of the PCB generated by the tool to find if components have collision and produce a bill of material to find out total components cost.

Design and layout is an important factor, figure 20 shows us the recommended layout for high and low current paths, ideally the low current circuit must share an small track ground interconnect for ground reference. Figure 21 is the final layout, the schematic can be found in the appendix, we considered in our design layout:

1. Majority of the passive components are chosen to be surface mount as it takes less space compared to through hole.
2. Usage of bottom and top plane copper stitched with multiple vias to allow for a high current flow from battery to load.
3. Optimised layout for chips, the AFE and the micro-controller are both centralised.
4. We added vias on around the perimeter of the PCB to stitch the ground planes to get as close to true ground

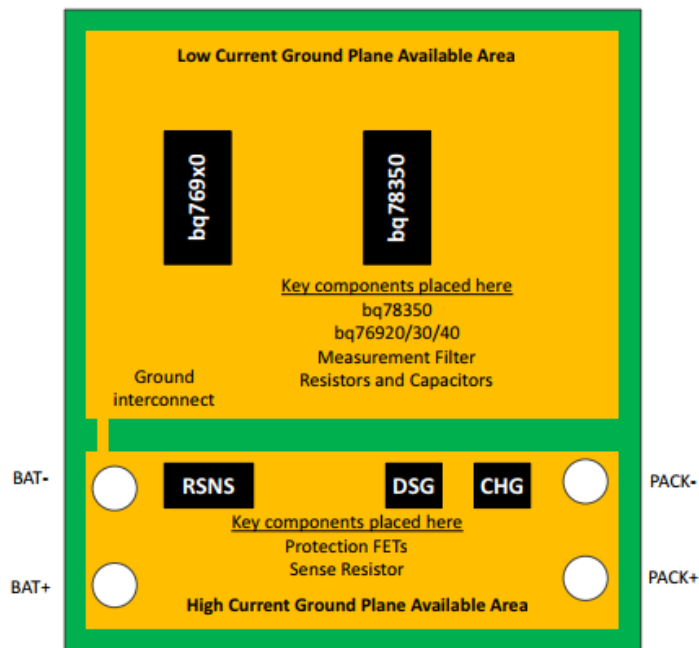


Figure 20: Recommended PCB Layout

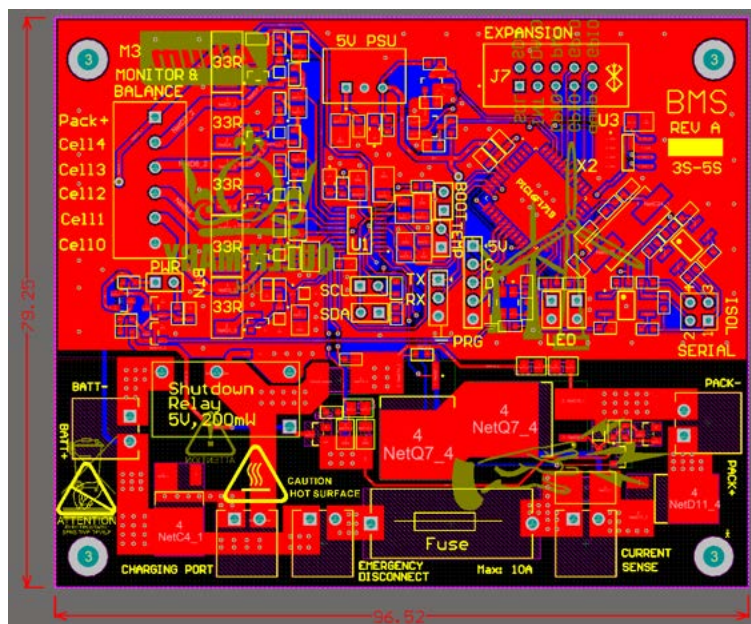


Figure 21: PCB Layout in Altium

### 5.5.2 Current Sensing Resistor for Coloumb Counting

Monitoring current is essential to provide protection and understand how much work the battery is doing, we use current to find the SOC which we employed in our firmware, also we can determine if the battery pack is being charged based on polarity of current flow. In figure 22 we use a differential matched filter network to a shunt resistor, the values for resistor and capacitor are chosen to filter out high frequencies. The current flowing through the resistor can be found based on the  $V=IR$  formula where the resistor is known and differential voltage across the resistor is read. Choosing the component is just as important as designing the circuit in our design we have considered:

1. Resistor temperature drift co-efficient (ppm/°C).
  - (a) Chosen resistor has a 70PPM/°C which means that for every degree there will be a change of 0.000070 ohms difference. If we work with full range of temperature of  $\Delta T = 50$  we a change of resistance to be  $0.000070 * 50 = 0.0035$  ohms.
2. High power rating 2W.
3. Current measurement over a large range can be done based on the choice of resistance, for our specification we have a range from 0 to 10A, with  $2^{14}$  levels.
4. Precision resistors have a low tolerance of 1% or lower. The typical resistor may have between 5% to 10% tolerance.
5. ADC precision and accuracy. The precision is based of the number of bits there are in the Analog to digital converter, in the AFE we have a precision of 14bits ADC.
6. Low impedance PCB track to reduce additional tolerance, this is a PCB design consideration.
7. Time sampling is also another factor if we have a higher time table we can achieve a better resolution of SOC.

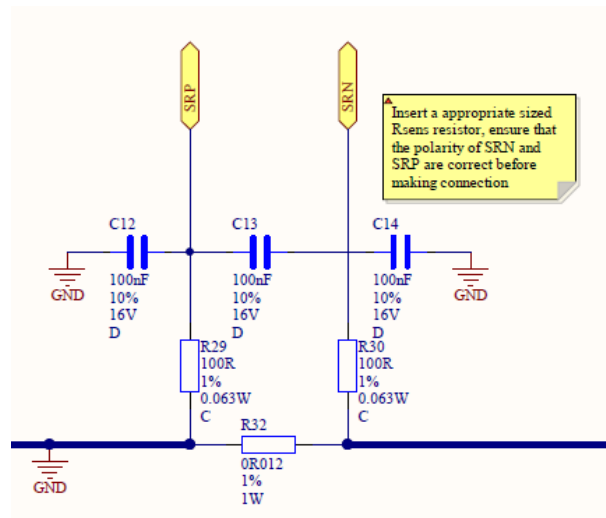


Figure 22: Current Sense Resistor Circuit with Filtering

### 5.5.3 High Power Cell Balancing and Voltage Monitoring Circuit

Cell balancing is an important feature which not all BMS include, it involves actively loading a single cell to prevent it from being overcharged, the cell chemistry can be severely affected even if overcharged by 0.05V. We use control this circuitry in software when the analog to digital converters read a certain threshold for overcharged voltage. The cell being balanced is effectively loaded and  $\approx 130\text{mA}$  flows through the dummy load via a N-channel MOSFET, the N-channel MOSFET used in this circuit has a lower operating  $v_{gs}$  voltage an zener diode at the gate is added for protection.

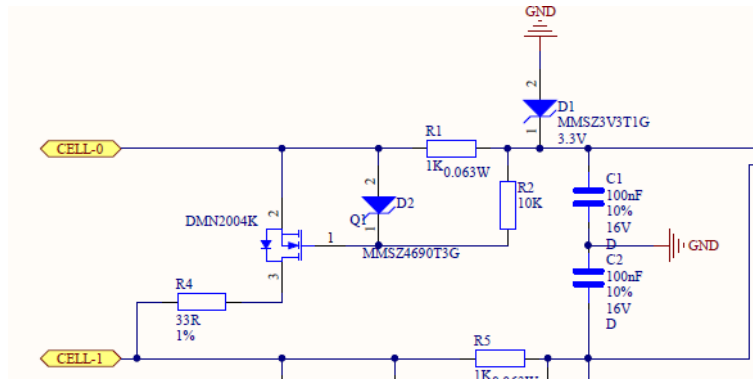


Figure 23: Cell-balancing & Monitoring

#### 5.5.4 Safety Battery Disconnect using Charge & Discharge Mosfets

The circuit presented uses two N channel mosfets (Q7 and Q8) seen in figure 24 driven by low side FET drivers to permit current flow in certain direction, mosfet Q7 enable the battery to source current to the load which is controlled by the BQ76920 analog front end discharge pin, a similar approach for enabling charging process is done for mosfet Q8. Q8 has additional circuitry to prevent high voltage damage to the analog front end charge pin, protection mosfet Q6 deals with the uncertainty due to floating voltage reference and case when VSS falls below 0V.

One downside with this feature is that the control is done by the analog front end, if the chip hangs or locks up then it may not react to provide safety when needed, we resolve this issue with other safety systems in the next sections.

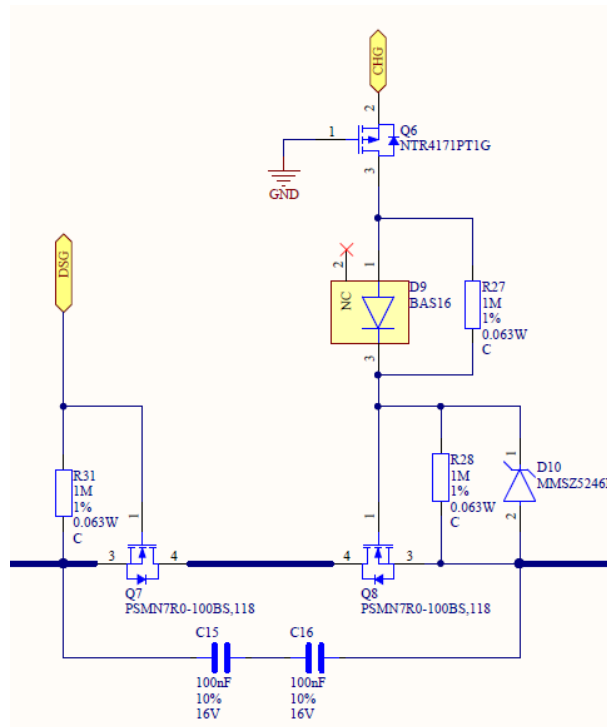
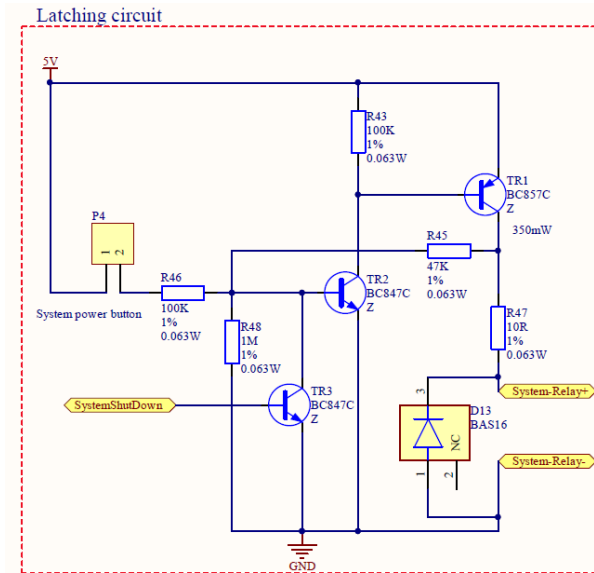


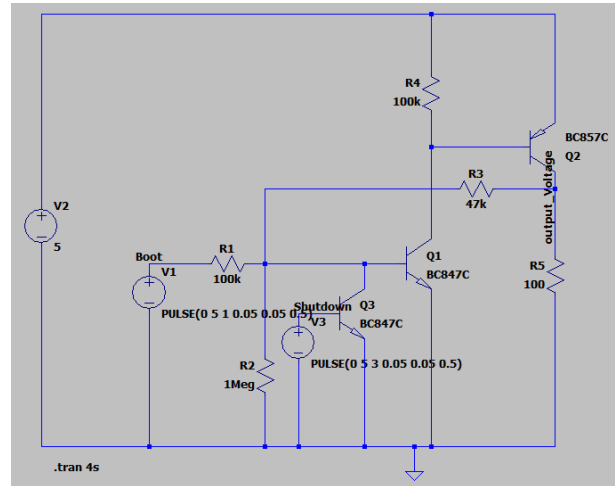
Figure 24: Charge & Discharge Mosfets

### 5.5.5 Safety Shutdown Latching Circuit

We have shown earlier on a few safety features which are employed to protect the batteries those include fuses, this system shuts creates an open circuit during catastrophic failure. What differentiate this safety features with others is that the signal to shutdown comes from the micro-controller, there are many states where there can be faults that would result in complex circuitry to detect but filtering out faults and making decision can be done digitally. Figure 25.(a) shows an simple latching circuit with an input to BJT (TR3) from an micro-controller pin.



(a) Latching circuit hardware design



(b) Latching circuit in simulator

Figure 25: Latching Circuit

We know that the circuit performs as designed through testing in simulation, the same circuit is replicated which is seen in figure 25.(b). The main purpose of this circuit is that the battery bank will be connected when the system is booted, once booted the battery will remain connected, this is latched. To describe circuit operation, initially there is an high signal from on base of TR2 from 'booting', this can be seen on the green signal in figure 26 which indicates momentary pulse. Once booted there will be a voltage output on the load which drives a latching relay, we use a low current signal to drive high power line. Using figure 25.(a) as reference, the circuit latches as current can flow through the base of TR1 to ground via TR2, a voltage now appears on the collector on TR1 and forms a feedback path to transistor TR2 effectively holding the base high.

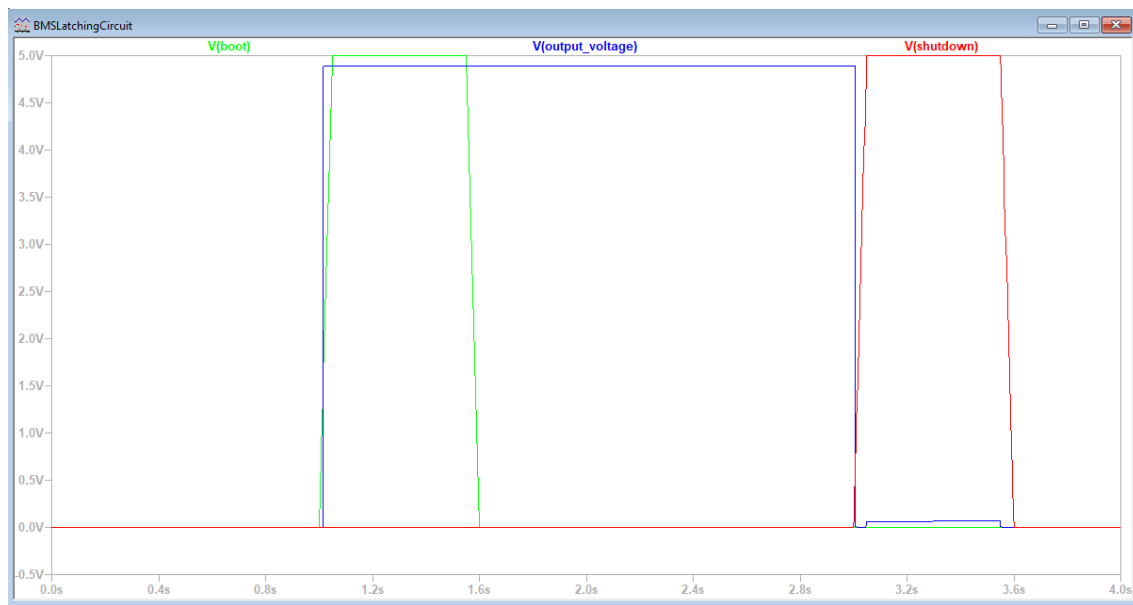


Figure 26: Latching Circuit Simulation Results



## 6 Testing & Results

### 6.1 Simulation results

A real wind profile sampled obtained from Loughborough wind farm databased is used as input for the simulated wind turbine. A 90 second simulation in Matlab/Simulink is carried out to test the system with and without a battery storage, the product of the simulation result is based on our system specification. The simulation result can be seen in the figure below:

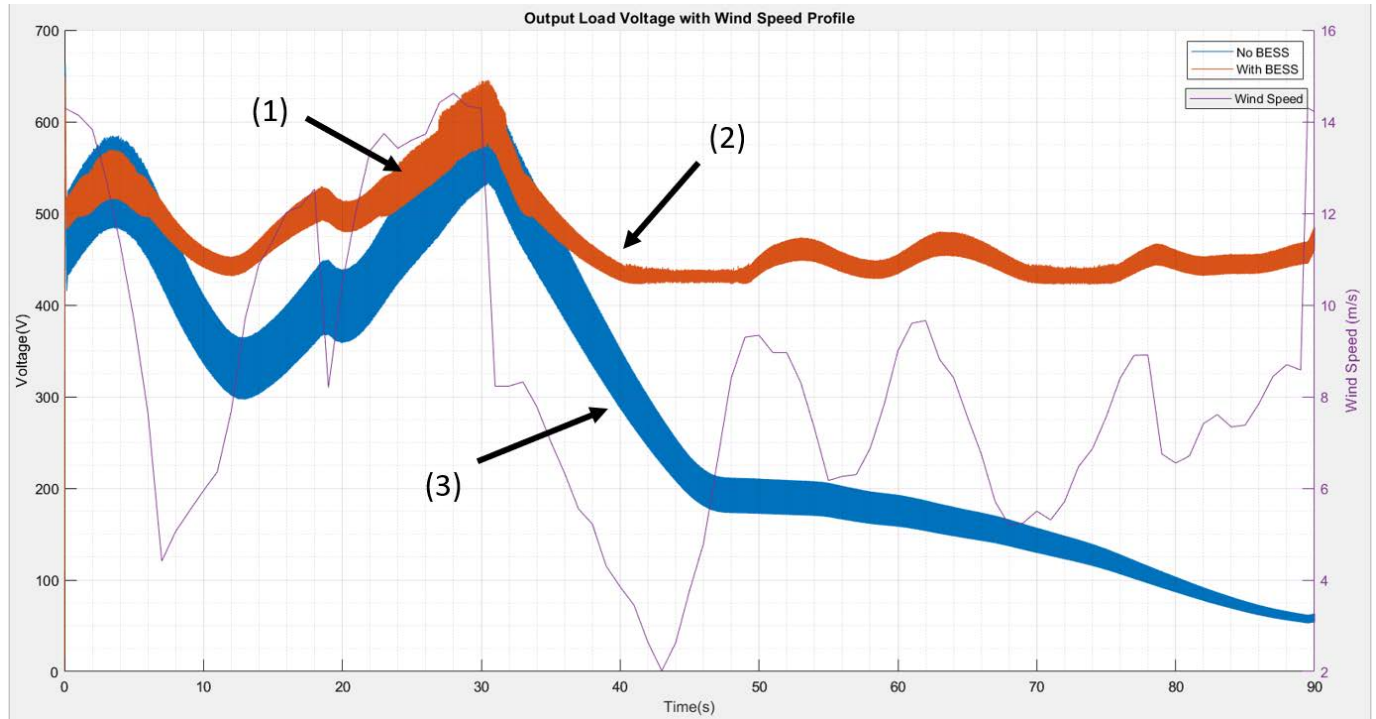


Figure 27: Simulation results using real wind profile

The simulation produces interesting results we can first analyse the standard deviation, this is used to determine how spread out the voltage variation is away from the mean, a low standard deviation mean is important as this shows that the peak to peak voltage is smaller.

The average voltage over the duration of the 90 second simulation is shown in figure 28, the results produced are significant we can also see the plot of standard deviation with the error lines, it proves that battery bank improves with smoothing out the voltage peak to peak. The standard deviation for No BESS is  $\approx 164$  while for BESS  $\approx 45$ , we compute that there is  $\approx 70\%$  reduction in peak to peak voltage with the battery bank is connected.



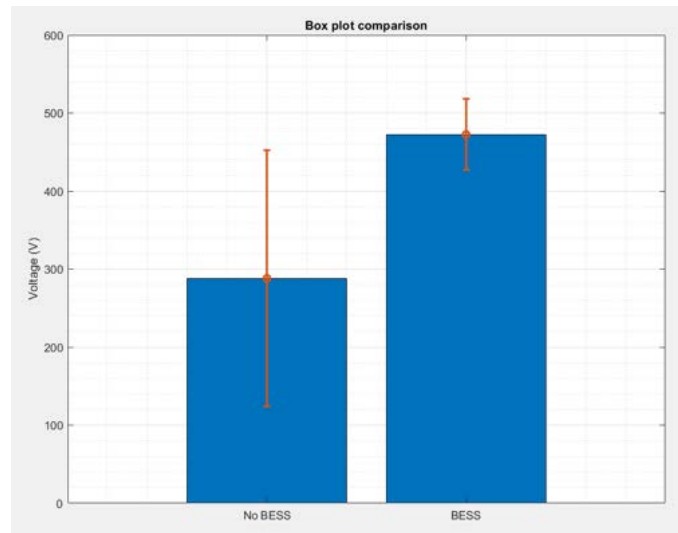


Figure 28: Simulation results using real wind profile

Make the axis font size bigger to be readable

Discussion about the points on graph 27:

Figure 27.(1) - Charging takes place when the wind turbine is able to supply voltage greater than the BMS threshold voltage (in this design it is set to 480V). At a high wind speed of 14 m/s in this simulation we can see that we have a limitation of the proposed system, the cause of this is that the bi-directional converter works outside its operational range. In this simulation we have the voltage generation as high as 650V at higher wind speed, this is expected because we have no feedback system such as pitch control to regulate the voltage generation.

Figure 27.(2) - If the cut-out speed does not last that long the battery bank can support the grid momentarily preventing the disconnection with the grid. We can see on the graph that at time 50s the wind speed begins to pick up again and the bi-directional converter switches to buck mode (charging) as voltage generated is greater than minimum threshold, with the battery energy storage system the voltage does not drop below 400V across our 90s time interval. The wave form compared to without BESS shows a less overall fluctuation over the duration of simulation time, thus the power output is more steady and closer to constant.

Figure 27.(3) - Without an battery storage system, when the voltage generation of the wind turbine falls below a certain point it cannot supply for the DC to AC converter, this will lead to de-synchronization of the wind turbine with the grid. This is the typical result of wind turbine output when the wind speed falls below the cut-out speed.

Now we can analyse how the SOC of the battery bank varies with voltage being read, this is seen on figure 30. During our time of simulation the battery bank appears to behave as we expect, when there is a surplus of voltage being generated indicated at figure 30.(1) the SOC initially plateaus then momentarily increases indicating charge. As the voltage begins to drop around the 40s mark, SOC decreases indicating that the battery bank is active. With the supplied wind profile, we can observe that the overall result at the end of simulation shows SOC being depleted slightly, our battery bank has drained more than being charged and maintained.

## 6.2 Limitation of the simulation model

From our defined specification the BMS threshold set at 480V, when the bi-directional converter is enabled to support the low voltage generation an issue arises. At the point of threshold when battery is connected there is oscillation about the 480V mark we can see this in Figure 29.(1)(2). Due to the lack of voltage

hysteresis, the battery system appears to be connected and disconnected at every instance when voltage drops below 480V indicated in figure at (2), this effect is undesirable and it induces more harmonics, this can be an low effort improvement which can be fixed by introducing hysteresis.

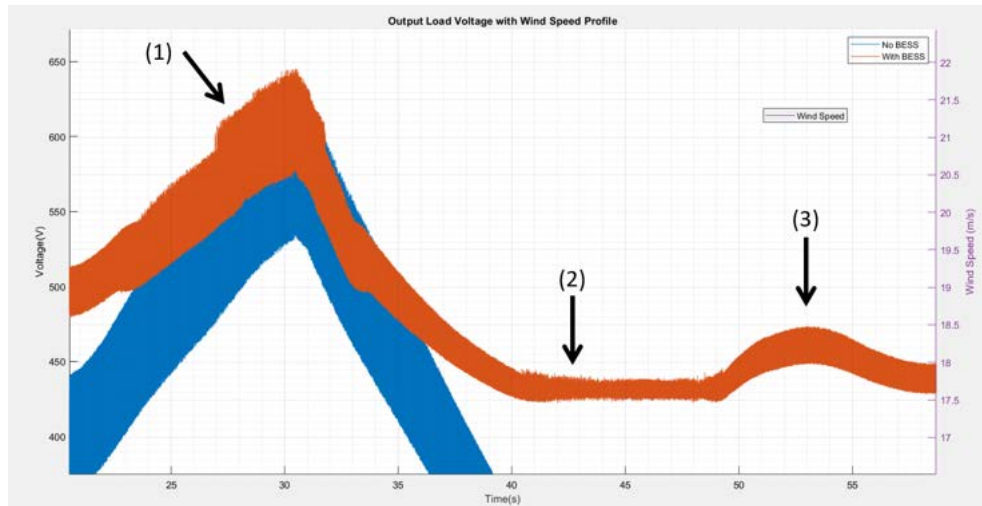


Figure 29: Occurrence of coarse oscillation

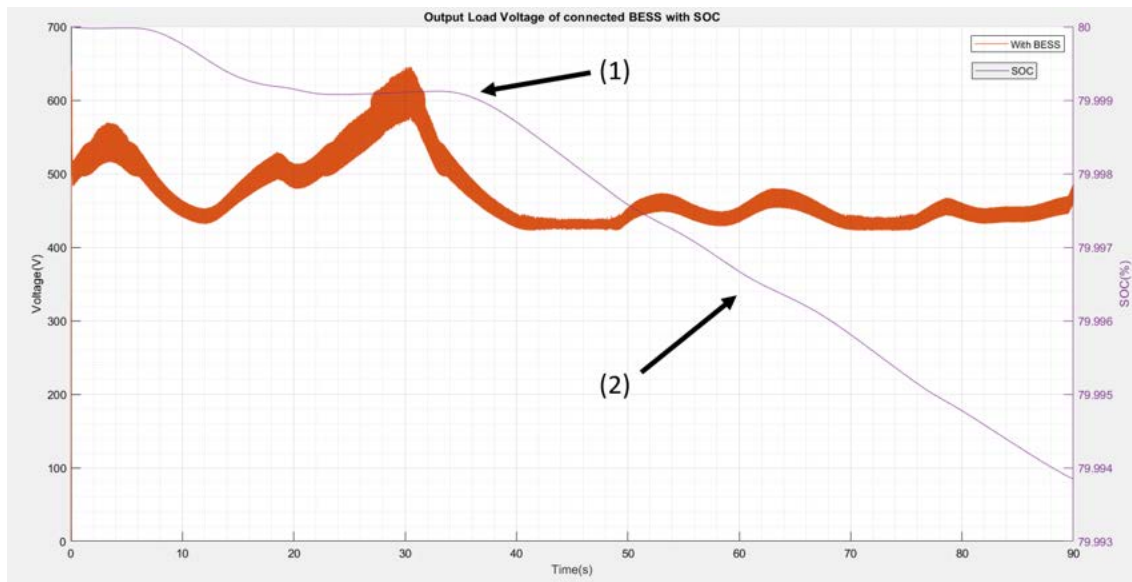


Figure 30: SOC of battery bank with varying wind speeds

### 6.3 Testing the BMS

A GUI was designed to preview the data sent from the BMS seen in figure 31, the data is sent as an CSV stream and is read using the serial USB port on a computer. We use a GUI development tool known as Processing which can create quick interfaces programmed in JAVA[19], we send a large amount of data elements from the BMS in CSV format.

During our real time display we test if our BMS is reactive, we can see that the on the live green lined graph when we change test the thermistor we get a new value for temperature, we also read all the SOC values from the cells which can be seen representatively as a level indicator, information about the registers such as under voltage, over current and short circuit can be read within the console box. From the results of

testing, we can conclude that majority of the BMS intended features are functioning as properly, we discuss what features have not been tested/developed in the conclusion section.

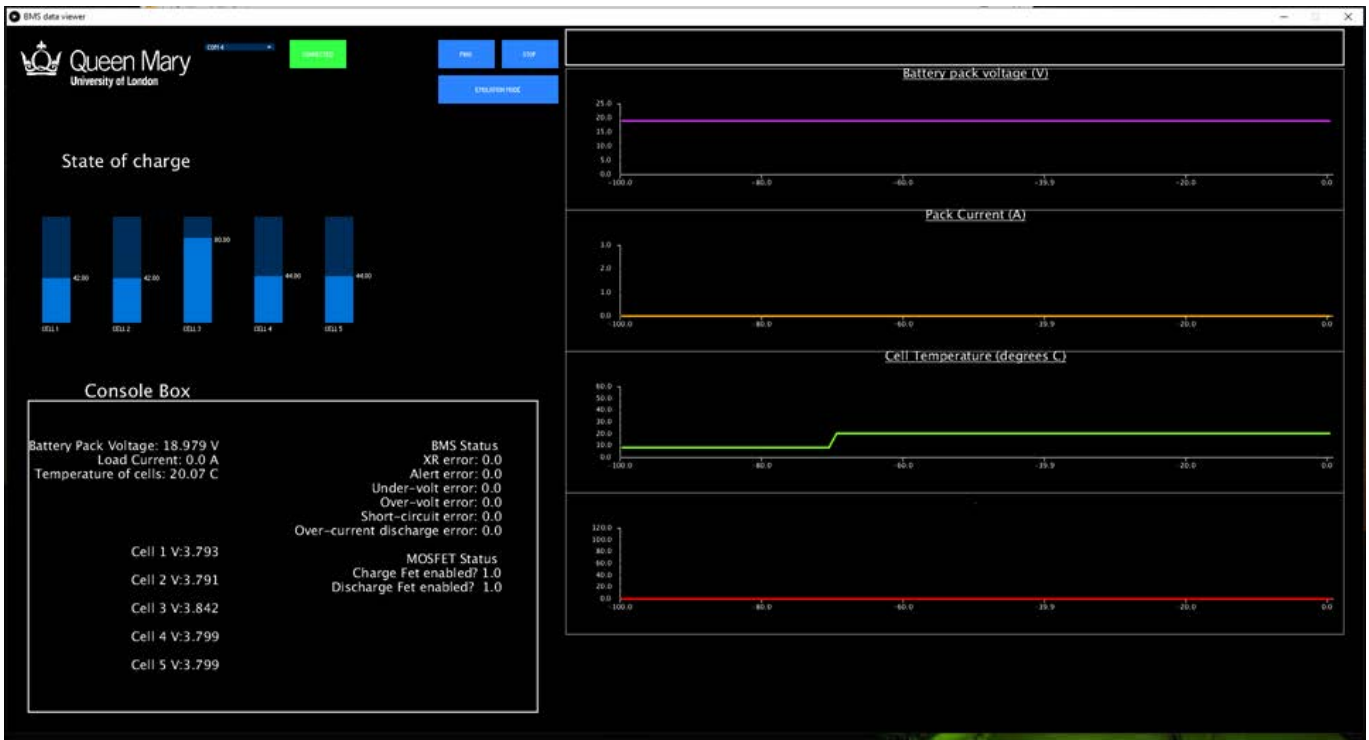


Figure 31: Viewing data on GUI from BMS

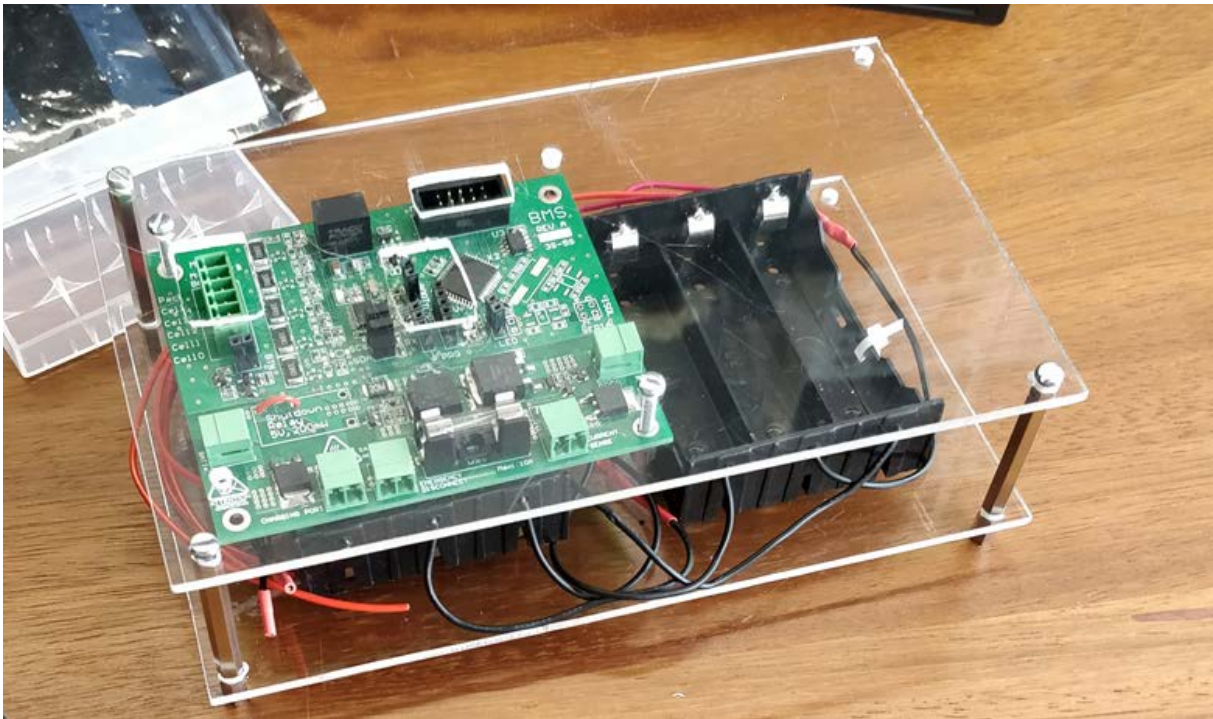


Figure 32: Hardware Demo & Prototype

### 6.3.1 Testing the thermistor

With the co-efficient calculated for our Stein-hart & Hart equation we tested the thermistor under different temperature conditions. We can verify that the thermistor on the BMS is working as intended as seen in figure 33, where the plot of sampled readings overlap with simulated curve, the degree of accuracy is high with the maximum  $\Delta$  resistance value being only  $\pm 10\Omega$ . For our test we have more resolution around the ambient temperature range of 20C - 25C, we have attempted to obtain more samples at the extremes but lack the proper equipment to do so.

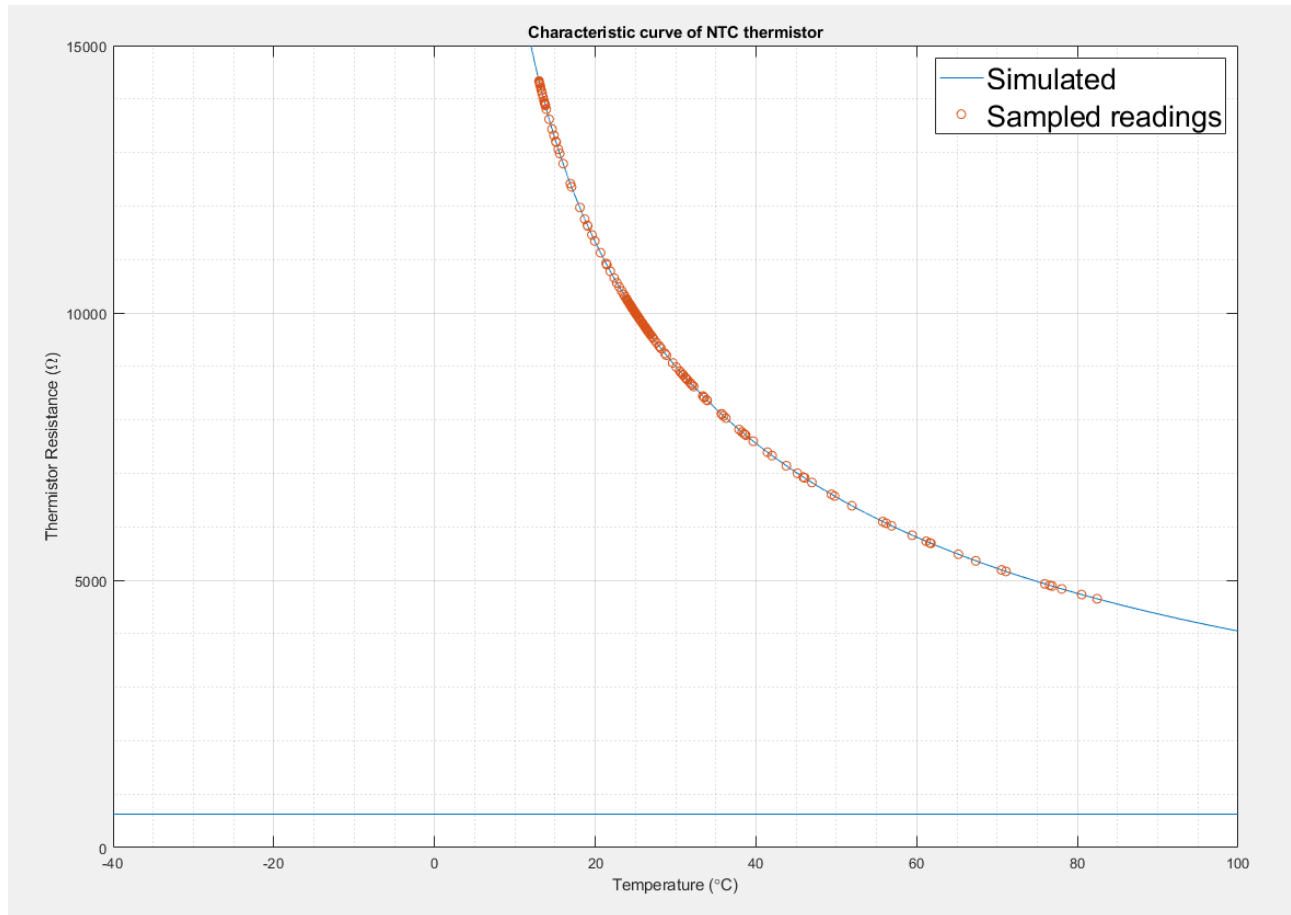


Figure 33: Simulated vs Sampled data readings

## 7 Conclusion

We had defined our specifications in the earlier BMS design section, we conclude with the table 8 to review what we have achieved in our BMS design. The basic feature 'cell balancing' feature has not yet been implemented, the factors for this include a combination of software and hardware complexities, the circuit includes both selection of low and high power cell balancing which is controlled by registers within the AFE, to program this requires more time.

| BASIC  | ACHIEVED? | UNIQUE   | ACHIEVED? |
|--|-----------|--|-----------|
| Pack over-current in discharge                       | Y         | State machine with low latency interrupt to protect battery bank as fast as possible   | Y         |
| Pack short circuit in discharge                      | Y         | Precise temperature measurement technique using Steinhart & Hart equations   | Y         |
| Cell under-voltage protection                        | Y         | Battery unloading and periodic SOC measuring via lookup table in EEPROM to re-calibrate estimated SOC  | Y         |
| Cell over-voltage protection                         | Y         | Watchdog timer to prevent communication lockup with BQ76920 analog front end chip  | Y         |
| Coloumb Counting                                     | Y         | Reporting status and battery information over isolated communication channel   | Y         |
| Monitoring individual cell voltages                  | Y         | PI controller to adjust charging voltage provided by bi-directional converter, PWM type control signal based on pack current and temperature | Not Yet   |
| Choice of low/high power cell balancing (50mA/150mA) | N         | -  | -         |

Table 8: BMS Requirements Met

## 8 Future Improvements

### 8.1 Simulation

Usually in practice bi-directional converters are controlled with a feedback system, in our simulation we have not implemented this as it works on open loop, adding feedback can help us stabilise the voltage and reduce the harmonics when charging the battery bank. If we were to add closed loop feedback, I would consider a PI controller and for initial tuning we can use Ziegler Nicholas tuning method.

### 8.2 BMS

SOC estimation algorithm in our BMS is not ideal, measurement is dependant on analog circuitry factors this can be estimation error caused by sensors proper calibration in practice can be expensive, we also update the SOC value when the battery pack is unloaded this may not happen that frequently and thus the error percentage increases with time. We should review other intelligent algorithms which can improve the estimation accuracy one such example could be the use Kalman filter, this algorithm uses series of

measurement over time to provide state prediction and measurement update. Kalman filter benefits from the information hidden in noise, source [20] suggests that they use linearisation parameters in their measurement equation and then applying Kalman filter to get an accurate SOC value, they concluded that estimation error is less than 0.5%. Another technique could include neural network estimation, source [18] suggest to use multiple weighted variables (previous SOC, time, current average, terminal voltage) which are put through a machine learning algorithm to recognise patterns.

## References

- [1] Mohammad A Abusara, Josep M Guerrero, and Suleiman M Sharkh. Line-interactive ups for micro-grids. IEEE Transactions on Industrial Electronics, 61(3):1292–1300, 2013.
- [2] Texas Instruments, Understanding the I2C bus. <<http://www.ti.com/lit/an/slva704/slva704.pdf>>, 2019. Accessed: 30-09-2019.
- [3] Tai C Yang. Initial study of using rechargeable batteries in wind power generation with variable speed induction generators. IET Renewable Power Generation, 2(2):89–101, 2008.
- [4] European Wind Energy Association. <<https://www.ewea.org/wind-energy-basics/faq/>>, 2019. Accessed: 10-10-2019.
- [5] GOV UK. Beis renewables statistics. PDF, 16-03-2018. Accessed: 10-10-2019.
- [6] Vestas v90 Manufacturer datasheet. <<https://en.wind-turbine-models.com/turbines/16-vestas-v90#datasheet>>, 2019. Accessed: 20-10-2019.
- [7] Randall, Tom - "Here's How Electric Cars Will Cause the Next Oil Crisis". <<https://www.bloomberg.com/features/2016-ev-oil-crisis/>>, 2016. Accessed: 20-10-2019.
- [8] Battery university, Secondary batteries. <[https://batteryuniversity.com/learn/article/secondary\\_batteries](https://batteryuniversity.com/learn/article/secondary_batteries)>, 2019. Accessed: 21-10-2019.
- [9] Battery university, How to monitor a battery? <[https://batteryuniversity.com/learn/article/how\\_to\\_monitor\\_a\\_battery](https://batteryuniversity.com/learn/article/how_to_monitor_a_battery)>, 2019. Accessed: 21-09-2019.
- [10] Tatsuo Horiba, T Maeshima, T Matsumura, M Koseki, J Arai, and Y Muranaka. Applications of high power density lithium ion batteries. Journal of Power Sources, 146(1-2):107–110, 2005.
- [11] Yuanyuan Fan, Megha Goyal, Arindam Ghosh, and Farhad Shahnia. Integration of wind energy conversion system with microgrid and utility. In 2014 Australasian Universities Power Engineering Conference (AUPEC), pages 1–6. IEEE, 2014.
- [12] Matthew T Lawder, Bharatkumar Suthar, Paul WC Northrop, Sumitava De, C Michael Hoff, Olivia Leitemann, Mariesa L Crow, Shriram Santhanagopalan, and Venkat R Subramanian. Battery energy storage system (bess) and battery management system (bms) for grid-scale applications. Proceedings of the IEEE, 102(6):1014–1030, 2014.
- [13] CN Bhende, Shivakant Mishra, and Siva Ganesh Malla. Permanent magnet synchronous generator-based standalone wind energy supply system. IEEE transactions on sustainable energy, 2(4):361–373, 2011.
- [14] Muhammad H. Rashid. Power Electronics: Devices, Circuits, and Applications 4th Edition, pages 250–270. Pearsons, 1988. Accessed: Dec-2019.
- [15] Battery university, How to prolong lithium based batteries? <[https://batteryuniversity.com/learn/article/how\\_to\\_prolong\\_lithium\\_based\\_batteries](https://batteryuniversity.com/learn/article/how_to_prolong_lithium_based_batteries)>, 2019. Accessed: 21-09-2019.
- [16] Vesta wind turbine 3D model. <<https://grabcad.com/library/wind-turbine-133>>, 2019. Accessed: 1-09-2019.
- [17] Samsung-INR18650 Lithium-ion cell. <<https://www.powerstream.com/p/INR18650-25R-datasheet.pdf>>, 2019. Accessed: 23-09-2019.

- [18] KGH Mangunkusumo, KL Lian, P Aditya, Y-R Chang, YD Lee, and YH Ho. A battery management system for a small microgrid system. In 2014 International Conference on Intelligent Green Building and Smart Grid (IGBSG), pages 1–6. IEEE, 2014.
- [19] Processing - Open-source graphical library and integrated development environment. <<https://processing.org/>>, 2019. Accessed: 21-12-2019.
- [20] Zhihao Yu, Ruituo Huai, and Linjing Xiao. State-of-charge estimation for lithium-ion batteries using a kalman filter based on local linearization. Energies, 8(8):7854–7873, 2015.



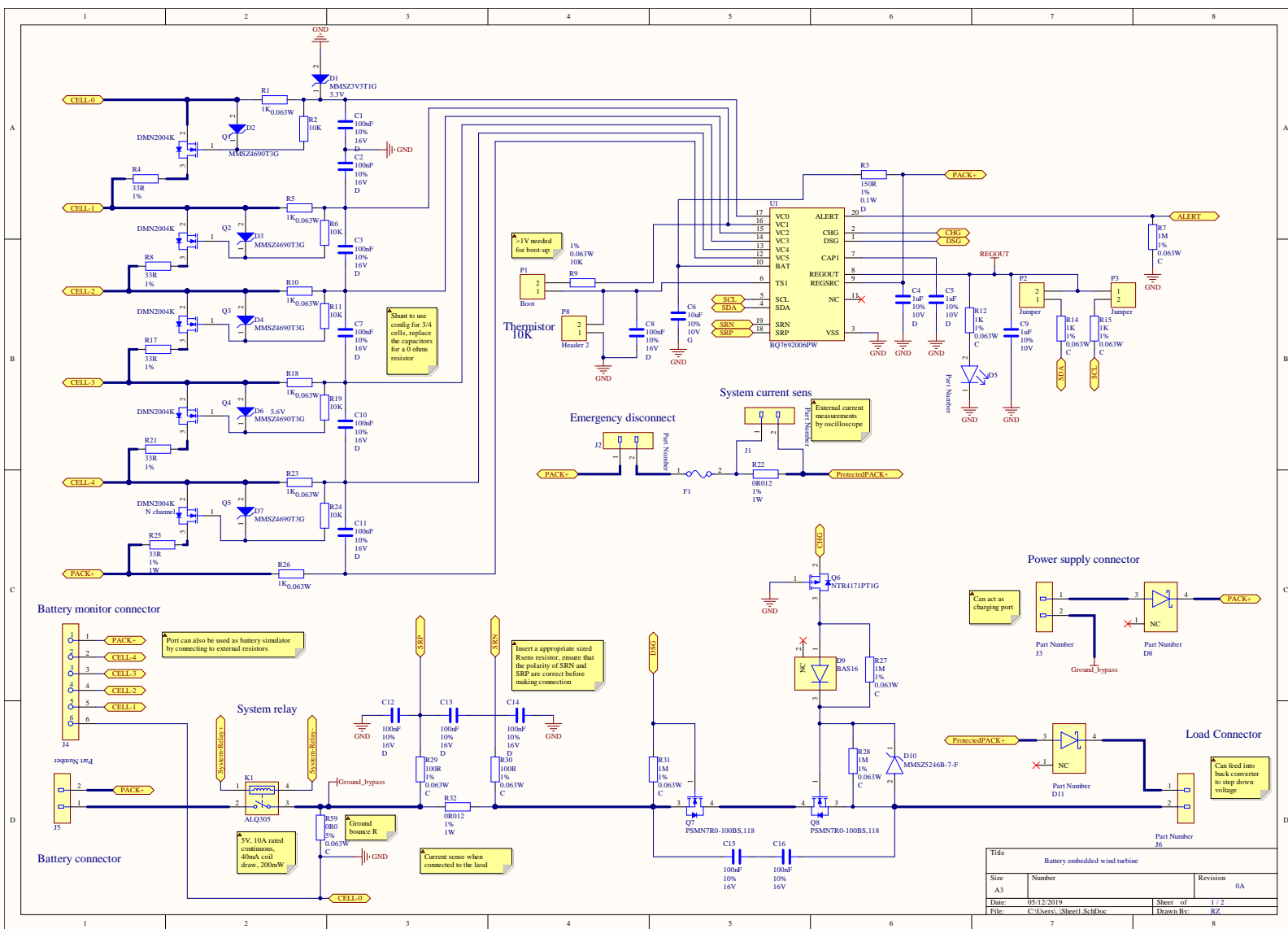
## **9 Appendix - A - Code**

The code for the BMS is located in the repository which be found:

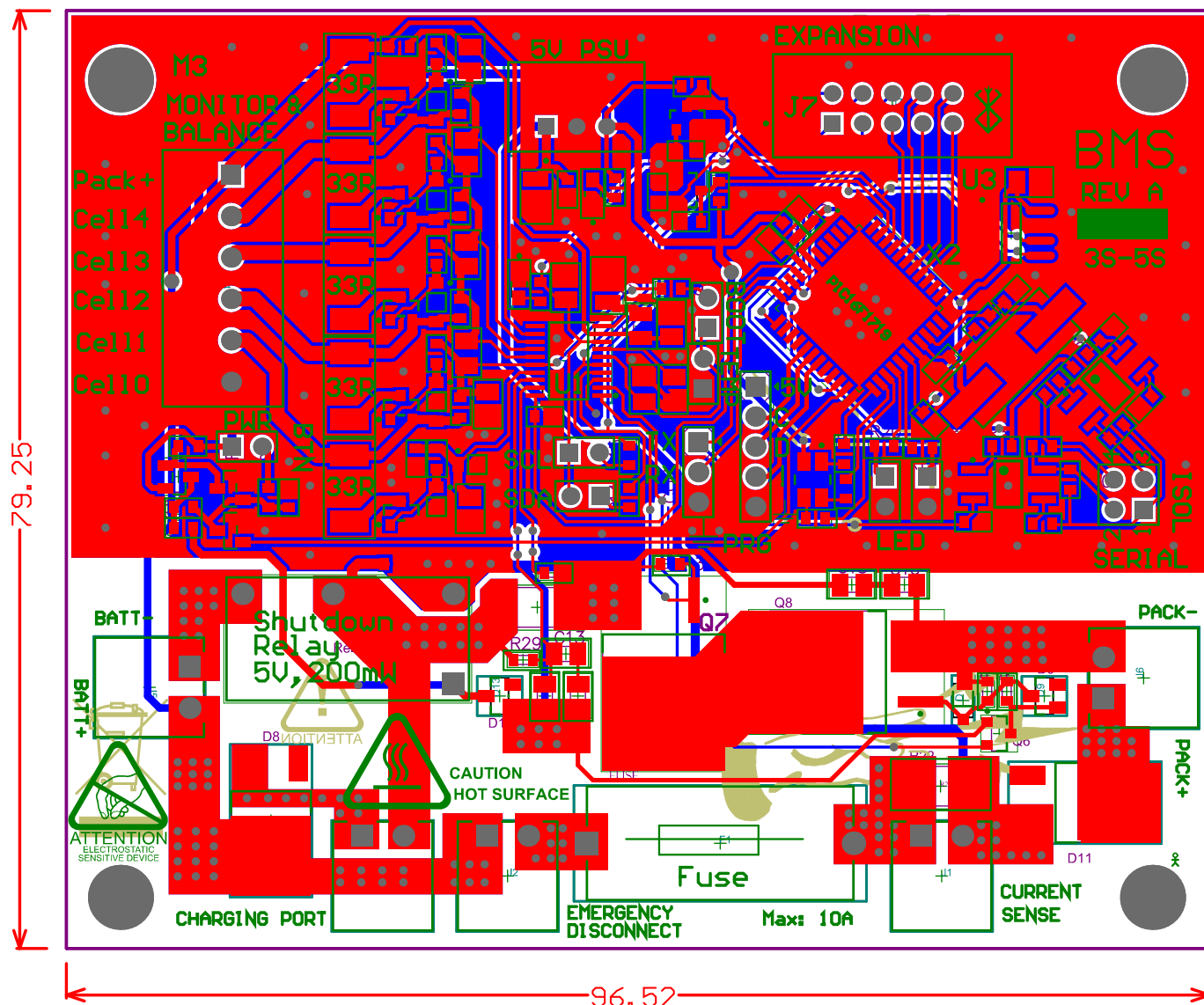
<https://github.com/raymond51/Embedded-Battery-Wind-Turbine>

## **10 Appendix - B - Schematic**

**Schematic**









make the image bigger to be readable

## 11 Appendix - C - Models

B

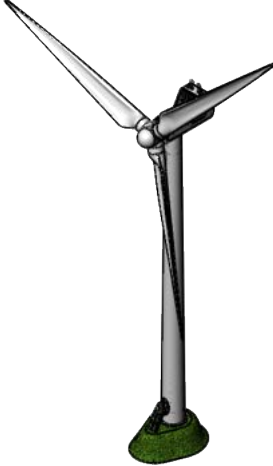
A

B

A

2

1



**PROPRIETARY AND CONFIDENTIAL**  
THE INFORMATION CONTAINED IN THIS  
DRAWING IS THE SOLE PROPERTY OF  
<INSERT COMPANY NAME HERE>. ANY  
REPRODUCTION IN PART OR AS A WHOLE  
WITHOUT THE WRITTEN PERMISSION OF  
<INSERT COMPANY NAME HERE> IS  
PROHIBITED.

|             |         |                             |           |      |      |             |              |
|-------------|---------|-----------------------------|-----------|------|------|-------------|--------------|
|             |         | UNLESS OTHERWISE SPECIFIED: |           | NAME | DATE | TITLE:      |              |
|             |         | DIMENSIONS ARE IN INCHES    | DRAWN     |      |      |             |              |
|             |         | TOLERANCES:                 | CHECKED   |      |      |             |              |
|             |         | FRACTIONAL ±                | ENG APPR. |      |      |             |              |
|             |         | ANGULAR: MACH ± BEND ±      | MFG APPR. |      |      |             |              |
|             |         | TWO PLACE DECIMAL ±         | Q.A.      |      |      | SIZE        | DWG. NO.     |
|             |         | THREE PLACE DECIMAL ±       | COMMENTS: |      |      | <b>A</b>    | <b>FYP</b>   |
|             |         | INTERPRET GEOMETRIC         |           |      |      | SCALE: 1:25 | WEIGHT:      |
|             |         | TOLERANCING PER:            |           |      |      |             | SHEET 1 OF 1 |
|             |         | MATERIAL                    |           |      |      |             |              |
|             |         | FINISH                      |           |      |      |             |              |
| NEXT ASSY   | USED ON |                             |           |      |      |             |              |
| APPLICATION |         | DO NOT SCALE DRAWING        |           |      |      |             |              |

1

2

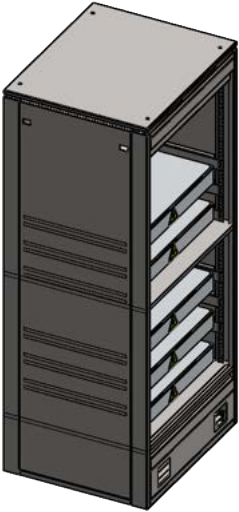
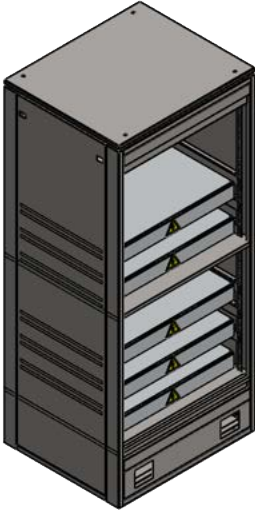
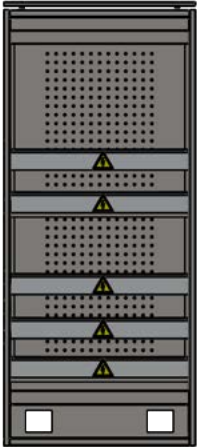
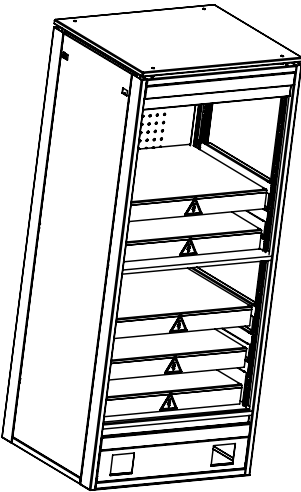
1

B

B

A

A



PROPRIETARY AND CONFIDENTIAL

THE INFORMATION CONTAINED IN THIS DRAWING IS THE SOLE PROPERTY OF <INSERT COMPANY NAME HERE>. ANY REPRODUCTION IN PART OR AS A WHOLE WITHOUT THE WRITTEN PERMISSION OF <INSERT COMPANY NAME HERE> IS PROHIBITED.

|             |         |
|-------------|---------|
| NEXT ASSY   | USED ON |
| APPLICATION |         |

UNLESS OTHERWISE SPECIFIED:

DIMENSIONS ARE IN INCHES

TOLERANCES:

FRACTIONAL ±

ANGULAR: MACH ± BEND ±

TWO PLACE DECIMAL ±

THREE PLACE DECIMAL ±

INTERPRET GEOMETRIC TOLERANCING PER:

MATERIAL

FINISH

DO NOT SCALE DRAWING

|           |      |
|-----------|------|
| NAME      | DATE |
| DRAWN     |      |
| CHECKED   |      |
| ENG APPR. |      |
| MFG APPR. |      |
| Q.A.      |      |
| COMMENTS: |      |

SIZE

DWG. NO.

REV

SCALE: 2:1

WEIGHT:

SHEET 1 OF 1

TITLE:

Battery Storage Unit 6-scale



## 12 Appendix - D - Misc

### Wind Turbine Model

#### Matlab code for computing values in Discharging mode

Listing 4: Computing Values for Required Specifications for Boost mode

```
1 input_v = 480;
2 average_output_V = 550;
3 Rload = 10;
4 p_p_v_ripple = 5;
5 switching_freq = 10000;
6 p_p_i_ripple = 5;
7 i_average = 50; %subject to change i believe its average load current draw in case of
   power failure
8
9 duty_cyle = 1 - (input_v/average_output_V);
10 fprintf('Duty cycle: %0.4f \n',duty_cyle);
11
12 inductor_value = (input_v * duty_cyle)/(switching_freq*p_p_i_ripple);
13 fprintf('Inductor value choice: %0.10d \n',inductor_value);
14
15 capacitor_value = (i_average*duty_cyle)/(switching_freq*p_p_v_ripple);
16 fprintf('Capacitor value choice: %0.10d \n',capacitor_value);
17
18 inductor_critical_val = ((1-duty_cyle)*duty_cyle*Rload)/(2*switching_freq);
19 fprintf('Inductor critical value choice: %0.10d \n',inductor_critical_val);
20
21 capacitor_critical_val = ((1-duty_cyle))/(16*inductor_value*(switching_freq).^2);
22 capacitor_critical_val = duty_cyle/(2*switching_freq*Rload);
23 fprintf('Capacitor critical value choice: %0.10d \n',capacitor_critical_val);
```

#### Matlab code for computing values in Charging mode

Listing 5: Computing Values for Required Specifications for Buck mode

```
1 % This solver provides values for inductor and capacitor values for buck
2 % converter design, the equations are derived from the rashid book pg.260
3
4 input_v = 690;
5 average_output_V = 480;
6 Rload = 10;
7 p_p_v_ripple = 10;
8 switching_freq = 10000;
9 p_p_i_ripple = 5;
10
11 duty_cyle = average_output_V/input_v;
12 fprintf('Duty cycle: %0.4f \n',duty_cyle);
13
14 inductor_value = (average_output_V*(input_v-average_output_V))/(p_p_i_ripple*
   switching_freq*input_v);
15 fprintf('Inductor value choice: %0.10d \n',inductor_value);
16
17 capacitor_value = (p_p_i_ripple)/(8*switching_freq*p_p_v_ripple);
18 fprintf('Capacitor value choice: %0.10d \n',capacitor_value);
19
20 inductor_critical_val = ((1-duty_cyle)*Rload)/(2*switching_freq);
21 fprintf('Inductor critical value choice: %0.10d \n',inductor_critical_val);
```

```

22
23 capacitor_critical_val = ((1-duty_cyle))/(16*inductor_value*(switching_freq).^2);
24 fprintf('Capacitor critical value choice: %0.10d \n',capacitor_critical_val);

```

## Matlab code for NTC thermistor characteristic curve

Listing 6: Steinhart and Hart Approach

```

1 %constants
2 Rt1= 2812.8;
3 Rt2= 2252;
4 Rt3= 1814.4;
5 T1= 20;
6 T2= 25;
7 T3= 30;
8 kelvinConst = 273.15;
9
10 a = [1 log(Rt1) log(Rt1)^3
11      1 log(Rt2) log(Rt2)^3
12      1 log(Rt3) log(Rt3)^3];
13
14 b = [(1/(T1+kelvinConst)) (1/(T2+kelvinConst)) (1/(T3+kelvinConst))]';
15 format long %store long decimal of co-efficient for better accuracy
16 x = (inv(a)*b)'; %transpose co-efficients
17
18 RTvar = linspace(0,15000,15000); %generate equal spacing resistance
19 maxSize = size(RTvar);
20 T=zeros(1,maxSize(1,2)); %initialise array with size of RTvar
21 %Compute value of T on every sample
22 for index = 1:(maxSize(1,2))
23     T(1,index) = 1/(x(1, 1)+x(1, 2)*log(RTvar(1,index))+x(1, 3)*log(RTvar(1,index))
24         ^3))-273.15;
25
26 end
27 %Plot graph
28 plot(T,RTvar)
29 xlim([-40 100])
30 xlabel('Temperature (\circ C)')
31 ylabel('Thermistor Resistance (\Omega)')
32 title('Characteristic curve of NTC thermistor')
33 grid on
34 grid minor

```

## Cell specifications

| Item   | Specification  |
|--|--|
| 3.1 Nominal discharge capacity                           | 2,500mAh<br>Charge: 1.25A, 4.20V, CCCV 125mA cut-off,<br>Discharge: 0.2C, 2.5V discharge cut-off                               |
| 3.2 Nominal voltage                                      | 3.6V   |
| 3.3 Standard charge                                      | CCCV, 1.25A, 4.20 ± 0.05 V, 125mA cut-off  |
| 3.4 Rapid charge   | CCCV, 4A, 4.20 ± 0.05 V, 100mA cut-off   |
| 3.6 Charging time  | Standard charge : 180min / 125mA cut-off<br>Rapid charge: 60min (at 25℃) / 100mA cut-off                                       |
| 3.7 Max. continuous discharge<br>(Continuous)            | 20A(at 25℃), 60% at 250 cycle  |
| 3.8 Discharge cut-off voltage<br>End of discharge        | 2.5V   |
| 3.9 Cell weight  | 45.0g max  |
| 3.10 Cell dimension                                      | Height : 64.85 ± 0.15mm<br>Diameter : 18.33 ± 0.07mm   |
| 3.11 Operating temperature<br>(surface temperature)      | Charge : 0 to 50℃<br>(recommended recharge release < 45℃)<br>Discharge: -20 to 75℃<br>(recommended re-discharge release < 60℃) |
| 3.12 Storage temperature<br>(Recovery 90% after storage) | 1.5 year -30~25℃(1*)<br>3 months -30~45℃(1*)<br>1 month -30~60℃(1*)  |

Figure 34: Samsung INR18650 Nominal specification datasheet

make the image bigger to be readable